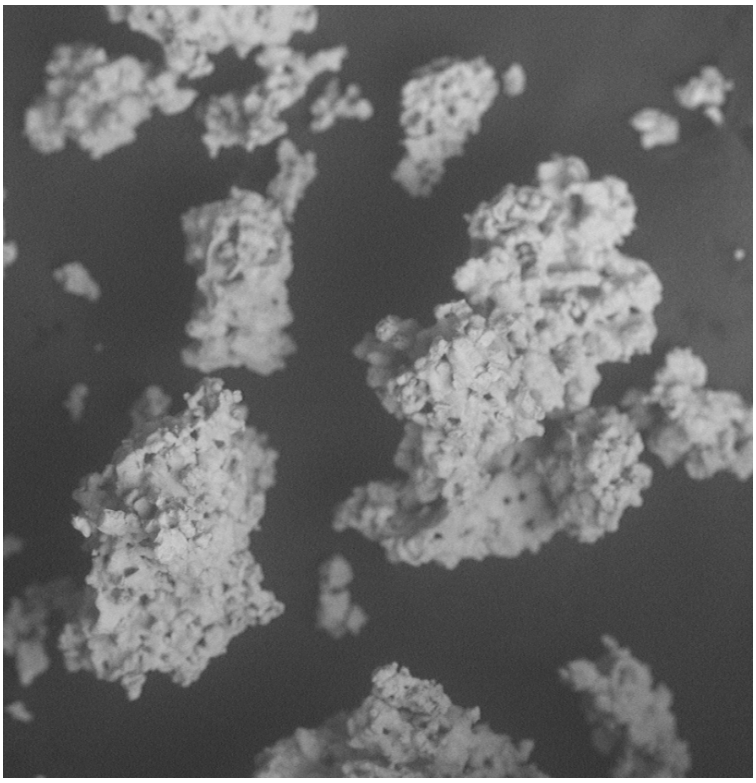

Synthesis and Characterization of Metal Oxide Energy Storage Materials

Evaluation of Thermochemical Energy Storage Materials Suggested from a Hybrid Data-Mining Approach

Master's thesis in Materials Chemistry

HAMPUS DAHLBERG*
WALDEMAR HULT

DEPARTMENT OF CHEMISTRY AND CHEMICAL ENGINEERING
CHALMERS UNIVERSITY OF TECHNOLOGY
Gothenburg, Sweden 2025
www.chalmers.se

Master's thesis 2025

Synthesis and Characterization of Metal Oxide Energy Storage Materials

Evaluation of Thermochemical Energy Storage Materials Suggested from a Hybrid Data-Mining Approach

HAMPUS DAHLBERG*
WALDEMAR HULT

CHALMERS
UNIVERSITY OF TECHNOLOGY

Department of Chemistry and Chemical Engineering
Division of Energy and Materials
Daniel Webers research group
Chalmers University of Technology
Gothenburg, Sweden 2025

Synthesis and Characterization of Metal Oxide Energy Storage Materials
Evaluation of Thermochemical Energy Storage Materials Suggested from a Hybrid Data-Mining Approach
HAMPUS DAHLBERG*
WALDEMAR HULT

Supervisor: Daniel Weber, Chemistry and Chemical Engineering
Examiner: Henrik Leion, Chemistry and Chemical Engineering

Master's Thesis 2025
Department of Chemistry and Chemical Engineering
Division of Energy and Materials
Daniel Webers research group
Chalmers University of Technology
SE-412 96 Gothenburg
Telephone +46 31 772 1000

Cover: SEM picture of calcium chromate ($CaCrO_4$) after it has been tested in a thermogravimetric analyser

Typeset in LaTeX
Gothenburg, Sweden 2025

Synthesis and Characterization of Metal Oxide Energy Storage Materials
Evaluation of Thermochemical Energy Storage Materials Suggested from a Hybrid Data-Mining Approach
HAMPUS DAHLBERG
WALDEMAR HULT
Department of Chemistry and Chemical Engineering
Chalmers University of Technology

Abstract

In this study, procedures for the solid state and sol-gel synthesis of metal oxides were developed for the purpose of thermochemical energy storage materials. The metal oxides or (blends of them) were suggested by Joakim Brorsson et al., in at the time of writing, unpublished research where he mines databases that fits the desired thermodynamical properties for thermochemical energy storage. Magnesium chromate, lithium aluminate, lithium chromate and calcium chromate where successfully synthesised by either one or both methods of synthesis, confirmed by X-ray powder diffraction. Barium Oxide had to be purchased from Sigma-Aldrich.
Utilising thermogravimetric analysis, a reference from was cuprous oxide was produced to compare observations on the metal oxide systems oxidation and reduction reactions. This data was utilised to calculate the systems conversion yield. Rough estimations of reaction kinetics of the systems where also utilised in comparison to the cuprous oxide reference. Calcium chromate and barium oxide where found to be good candidates for the application of thermochemical energy storage as the chalcium chromates, made through solid state synthesis, weight changed by 8%, and the barium oxides' weight changed by 10%.

Keywords: thermochemical energy storage, solid state synthesis, sol-gel synthesis, metal oxide oxygen carriers

Acknowledgements

We want to thank Henrik Leion, for him taking up the task of being our examiner and giving us the opportunity to write our master thesis. A greater thanks is extended to our supervisor Daniel Weber for his input on synthesis method, XRD analysis and consultation. Further gratitude is extended to the members of the Daniel Webers research group for their acts of assistance and Pontus Ericstam for accepting the delegated work of booking and running XRD according to our needs. Without these people´s help this work would not have been completed in a timely manner.

Hampus Dahlberg, Waldemar Hult, Gothenburg, June 2025

List of Acronyms

Below is the list of acronyms that have been used throughout this thesis listed in alphabetical order:

CLOU	Chemical looping with oxygen uncoupling
CSP	Concentrated solar power
OC	Oxygen carrier
PXRD	Powder X-ray diffraction
SEM	Scanning electron microscopy/microscope
TCHS	Thermochemical heat storage
TGA	Thermogravimetric analysis
THS	Thermal heat storage
XRD	X-ray diffraction

Contents

1
Introduction

1.1 The Need for Energy Storage in Concentrated Solar Power

The demand for sustainable energy sources are ever increasing under the threat of climate change. Concentrated solar power (CSP) is one possible part of the solution, but has the downside of being reliant on weather conditions and time of day to generate power. This intermittence causes gaps in the electricity available to power homes and industries.
Therefore there is a need to store excess energy production that is unutilised. Batteries offer one way to do this by storing and releasing generated electricity, but at a high cost for large scale applications. Since a CSP facility already has the equipment to convert thermal energy to electricity, a cheaper option is to store excess thermal energy directly. That way electricity can be generated during periods of downtime or when demand/costs are high or there are no other alternatives available.[1]

One of the main principles of power generation is that higher temperatures lead to greater thermal efficiency in power cycles, such as the Rankine cycle. The biggest advantage of CSP are the ranges of temperatures that are possible to operate on, depending on the configuration. Solar furnaces can reach temperatures up to 3500°C[2] while solar power towers can operate up to 1350°C.[3] Aside from CSP being intermittent this leads to it's second largest drawback: the medium in which the thermal energy is stored sets its operating temperature.

1.2 Thermal Energy Storage, Operating Temperatures, Desirable Characteristics And The Basis For This Study

There are three thermal energy storage categories that are applicable for CSP. Sensible heat storage, latent heat storage and thermochemical energy storage which will be briefly elaborated on.

Sensible Heat Storage is based on the principle of utilising a material's heat capacity (kJ/kg*K). The material can be heated up and then later cooled as needed to store or utilise the harvested energy, without a phase change.
Water with its liquid heat capacity 4,19 kJ $kg^{-1}K^{-1}$ or concrete gravel with 0,9 - 1,3 kJ $kg^{-1}K^{-1}$[4] are safe and low cost examples of materials that can be used with CSP to store and utilise the generated heat but has low operating temperatures not exceeding 100°C and these facilities require large volumes on an industrial scale.[5]
A more compact alternative is molten salt energy storage which is the current most widely used thermal storage method in CSP. It works by melting salts based on nitrates, chlorides, fluorides and carbonates and pumping them to a superheated steam turbine facility to generate electricity. They are limited by both their energy density, decomposition temperature and corrosive properties This comes with safety concerns and limits the operating temperature to around 565°C, lowering their efficiency. [6]

Latent Heat Storage is based on the energy required for a phase transition to occur under close to isothermal conditions. The transitions can be summed up in liquid to gas, liquid to solid or solid to gas or vice versa. The energy density of latent heat storage is much higher. For examples it takes 334 kJ to freeze one liter of water. The same amount of energy used to heat it would take it to 79.9°C. The conversion from liquid to solid is especially favourable for thermal storage applications since the change in volume is small. Latent heat storage materials are collectivised under the name phase change materials and has been proposed in CSP but suffer major drawbacks with risks of leaking, poor heat conversion and low thermal conductivity, making them inefficient. [7]

Thermochemical energy storage (TCES) is a method to store thermal energy through reversible chemical reactions, rather than as sensible and latent heat.[8] The typically large energy used or released in chemical reactions can allow for a high density of stored energy. The energy can easily be stored for a long time, unlike heat, as long as the conditions for the energy releasing reaction are not met.
A type of reaction suited well for TCES, and the one that will be the scope of this study is the partial reduction of a metal oxide (oxygen carrier (OC)) at high temperature in a low oxygen atmosphere and the exothermic oxidation in air back to the original species. This is due to the conditions for an OC to oxidise or reduce is mainly dependent on the partial pressure of oxygen or a high enough temperature. This allows for the thermal energy to be stored chemically in the reduced oxygen

carrier, that can later be oxidised to release it once again as heat. [9] [10]

For this to work the excess oxygen has to be released as O_2 without need for a separate substance to be reduced. This condition is also necessary for a more researched process called chemical looping with oxygen uncoupling (CLOU), a variant of chemical looping combustion (CLC) in which the oxygen carrier is used to separate pure oxygen from the atmosphere for an oxy-fuel combustion. Furthermore an oxygen carrier both in TCES and CLOU need to withstand cycling. Depending on configuration of the reactor (fixed bed, fluidised bed etc.) this means that OC particles should not conglomerate, nor disintegrate. [9] [10]
For the application to be practical, the oxygen carrier needs to couple and uncouple oxygen fast enough. This means that the reaction kinetics must be sufficiently fast and that the oxygen carrier either needs good oxygen diffusivity or a large surface area. The materials also need to be able to withstand the high operating temperatures of the processes they are to be applied for. The desired characteristics of the storage is a good energy density (kWh/m^3), efficiency and economical viability and when it comes to CSP, a high melting point to avoid agglomeration and attrition. [11]

One of the biggest challenges with research in general is the resource cost of it. A soft division of relevant costs can be summarised in time, labour, reactants, equipment and opportunity. The guess work involved rely most often on current topic trends and the researchers' intuition to pick a subject/potential material and then do the work required. It comes with great risks and rewards depending on the results and conclusions.
To mitigate these risks, there is a need for tools that reduce insecurity in addition of adding guidance and validation to the researchers proposal. An additional bonus would be that these tools sometimes could suggest materials that would go unnoticed due to ignorance or bias. One such tool are computer simulations and calculations.

In an article published in the journal of physical chemistry a group of researchers used the energetic data retrieved from the Open Quantum Materials Database to find potential candidate OCs for the application of CLOU[12]. In an (at the time of writing) unpublished follow up article currently named "Discovery of thermochemical energy storage materials via a hybrid datamining approach" Joakim Brorsson et al. has applied the same principle in an attempt to find candidate materials with characteristics fit for TCES research. [13]
The main points that this study will focus on to select candidates from the provided list are the equilibrium temperature and reaction enthalpy of a system to pick candidates. The current list that was provided can be seen in Table 1.1 and will most likely change before publication.[13]

As a result the main objective of this study is to synthesise some of these candidates, determine the ease of synthesizability of the systems and observe their oxygen uncoupling capabilities to evaluate Brorsson´s methods. Systems contain sodium where

excluded due to its tendency for agglomeration and low melting point. Caesium and rubidium were excluded due to their high costs.

Table 1.1: The top 30 filtered transitions with the highest reaction enthalpy from a draft of [13]

Place	Transition	Equilibrium temperature) (°C	Reaction enthalpy (kJ/kg)
1st	$\frac{2}{3}CaO + \frac{2}{3}CaCr_2O_4 + O_2 \rightleftharpoons \frac{4}{3}CaCrO_4$	1382.9	474.87
2nd	$2\,K_2O + O_2 \rightleftharpoons 4\,KO$	1353.1	348.98
3rd	$2\,Na_2O + O_2 \rightleftharpoons 4\,NaO$	756.1	345.50
4th	$\frac{4}{3}CaO + \frac{2}{3}Cr_2MgO_4 + O_2 \rightleftharpoons \frac{2}{3}MgO + \frac{4}{3}CaCrO_4$	1363.9	327.80
5th	$2\,Cu_2O + O_2 \rightleftharpoons 4\,CuO$	1375.6	298.19
6th	$\frac{2}{3}CaCr_2O_4 + \frac{1}{2}Ca_2MnO_4 + O_2 \rightleftharpoons \frac{4}{3}CaCrO_4 + \frac{1}{6}Ca_2Mn_3O_8$	1346.9	270.91
7th	$2\,BaO + O_2 \rightleftharpoons 2\,BaO_2$	628.0	264.37
8th	$CaCr_2O_4 + O_2 \rightleftharpoons CrO_2 + CaCrO_4$	1117.5	261.12
9th	$\frac{2}{3}MgO + \frac{2}{3}Cr_2MgO_4 + O_2 \rightleftharpoons \frac{4}{3}CrMgO_4$	512.2	260.62
10th	$\frac{2}{3}MgNa_6O_4 + O_2 \rightleftharpoons \frac{2}{3}MgO + 4\,NaO$	740.9	252.57
11th	$Cu_2O + 2\,VO_2 + O_2 \rightleftharpoons Cu_2V_2O_7$	1471.2	231.73
12th	$\frac{3}{4}CaCr_2O_4 + \frac{1}{2}Ca_2MnO_4 + O_2 \rightleftharpoons \frac{3}{2}CaCrO_4 + \frac{1}{4}CaMn_2O_4$	1356.3	225.58
13th	$\frac{2}{3}Cr_2MgO_4 + \frac{2}{15}Mg_6MnO_8 + O_2 \rightleftharpoons \frac{4}{3}CrMgO_4 + \frac{2}{15}MgMnO_3$	483.9	204.04
14th	$CrK_4O_4 + O_2 \rightleftharpoons 2\,KO + CrK_2O_4$	1294.1	200.35
15th	$2\,RbO + O_2 \rightleftharpoons 2\,RbO_2$	492.2	191.66
16th	$CuRb_3O_2 + O_2 \rightleftharpoons 2\,RbO + CuRbO_2$	1341.5	191.13
17th	$2\,Rb_2O + O_2 \rightleftharpoons 4\,RbO$	1372.1	184.57
18th	$\frac{4}{3}CuK_3O_2 + O_2 \rightleftharpoons 2\,KO + \frac{2}{3}Cu_2K_3O_4$	1294.8	183.54
19th	$\frac{11}{9}AlLiO_2 + \frac{11}{9}CrLiO_2 + O_2 \rightleftharpoons \frac{1}{9}Al_{11}O_{18} + \frac{11}{9}CrLi_2O_4$	900.9	178.62
20th	$\frac{4}{3}CaCr_2O_4 + O_2 \rightleftharpoons \frac{2}{3}Cr_2O_3 + \frac{4}{3}CaCrO_4$	1101.8	177.78
21st	$\frac{4}{5}Cu_2O + \frac{8}{5}VO_2 + \frac{4}{5}MgVO_3 + O_2 \rightleftharpoons \frac{2}{5}Cu_4Mg_2V_6O_{21}$	1509.7	177.00
22nd	$\frac{22}{39}Al_4CaO_7 + \frac{22}{39}CaCr_2O_4 + O_2 \rightleftharpoons \frac{8}{39}Al_{11}O_{18} + \frac{44}{39}CaCrO_4$	1154.1	176.80
23rd	$\frac{2}{3}BaNa_6O_4 + O_2 \rightleftharpoons \frac{2}{3}BaO + 4\,NaO$	734.7	175.93
24th	$\frac{2}{3}Cr_2MgO_4 + \frac{1}{3}Mg_2O_4Si + O_2 \rightleftharpoons \frac{1}{3}O_2Si + \frac{4}{3}CrMgO_4$	397.6	174.09
25th	$\frac{4}{3}Cr_2SrO_4 + O_2 \rightleftharpoons \frac{2}{3}Cr_2O_3 + \frac{4}{3}CrSrO_4$	1515.3	172.11
26th	$\frac{2}{3}CeRb_2O_3 + O_2 \rightleftharpoons \frac{2}{3}CeO_2 + \frac{4}{3}RbO_2$	411.0	170.35
27th	$2\,K_2MgO_2 + O_2 \rightleftharpoons 4\,KO + 2\,MgO$	1221.8	158.12
28th	$CrLi_3O_4 + CrLiO_2 + O_2 \rightleftharpoons 2\,CrLi_2O_4$	932.2	151.19
29th	$\frac{22}{39}Cr_2O_3 + \frac{88}{39}AlNaO_2 + O_2 \rightleftharpoons \frac{8}{39}Al_{11}O_{18} + \frac{44}{39}CrNa_2O_4$	1514.3	147.26
30th	$\frac{22}{39}Cr_2O_3 + \frac{44}{39}Al_2BaO_4 + O_2 \rightleftharpoons \frac{8}{39}Al_{11}O_{18} + \frac{44}{39}BaCrO_4$	1532.2	146.71

2
Theory

This chapter covers the theoretical basis of the experiments. Solid state synthesis, sol-gel synthesis, X-ray diffraction, thermogravimetric analysis, the degree of conversion, and scanning electron microscopy. In addition there is a short summary of the material's indsutrial backgrounds and if they have been previously studied for either CLOU or TCES.

2.1 Solid State ynthesis

Solid state synthesis is a material production method were reactants are mixed and then reacted together at specific high temperatures and times to form a new material and crystal structure. To achieve the correct synthesis there are a number of parameters to take into consideration. Particle size of reactants dictate how well the reactants are mixed since in this study no solvents are used. Other important factors include how densely packed the reactants are for the diffusion and crystalline growth of the product, precise stoichiometry of the reactants and choice of precursors (affects reaction kinetics), pressure, pre crystalline state (lattice constraints and crystalline evolution), reaction atmosphere and possible reaction pathways all affect the outcome of the synthesis. For a successful synthesis to occur these parameters need to be known and applied to get a pure crystalline phase [14], [15], [16], [17]

2.2 Sol-Gel Synthesis

Sol-gel stands for Solution-gel. One of the challenges with solid state synthesis is mixing of the reactants and it being limited by mass transport phenomena. This can to some degree be overcome by ball milling to reduce the powders particle size but getting pure phases remains a challenge and the process may require repetitions until a satisfactory quality is achieved. To overcome this sol-gel was developed. The process works by dissolution of precursor reagents into a colloidal system and by addition of a gelation agent creating a well mixed semi-solid (or polymeric) network referred to as a gel or gel matrix. One such gelation agent is citric acid which, when deprotonated, is able to form metal-citrate complexes through its $COO(-)$, groups. As water is evaporated from solution the citric acid creates a polymeric network, ensuring the metal cations and nucleation points are properly dispersed at an atomic scale and are able to grow evenly when the citrate is pyrolysed in an oxygen rich atmosphere. Burning off to CO_2, hopefully allowing for the correct phase pure metal crystals to form. [18]

2.3 X-Ray Diffraction

To verify the identity of the materials used, X-ray diffraction (XRD), more specifically powder x-ray diffraction (PXRD), was used. This non-destructive analysis method works by exposing the sample to X-rays at various inclinations and note how strongly they are reflected at different angles. This is dependent on diffraction effects from crystal structures in the sample and gives different compounds a highly unique diffractogram that can be used to identify them and indirectly identify the crystals constitutional elements when compared to online databases. This basic principle is used in this study to draw the conclusion if the method of synthesis was successful or failed since the constitutional elements are already known.[19]

2.4 Thermogravimetric Analysis

The simplest way to describe thermogravimetric analysis (TGA) is that it is a scale inside an oven, with a customisable atmosphere. The method allows to track weight changes in a material over a temperature, time range and a chosen atmosphere. This is useful because that means it is possible to track the thermal stability of a material when it starts to decompose, changes in the material and can be used to calculate the kinetics of the reactions with statistical methods if you know the probable reactions beforehand. These methods require different heating rates (ranging between 5-25 °C/min) and multiple high quality reproducible data sets.[20], [21]

2.4.1 Degree of Conversion

Aside from the importance of kinetics in a TCES material, an additional parameter that needs to be taken into account is to calculate how much of the sample that takes part in the redox cycle, which can be described by the term degree of conversion. This is important because the thermal energy is stored in the OC and if only 10% of the particle is cycling between phases the other 90% just takes up volume. This is necessarily not a downside for actual applications or for investigating parameters such as cycling life, but these factors aren't of interst in this work.

In summary there is a need to know how effetively the synthesised materials cycle in comparison to reference materials. The degree of conversion was calculated from the TGA results using this formula

$$\frac{n_O/\text{stoichiometric factor}}{n_{peak}} \tag{2.1}$$

where n_O is the moles of oxygen released from the sample during the TGA cycle and n_{peak} is the amount of substance of sample, calculated from the mass at the peak assuming total conversion to the oxidised right hand side of the equilibrium. The stoichiometric factor is the number of oxygen atoms released by one right hand side molecule (i.e. $CaCrO_4$, BaO_2 etc.) when transitioning to the more reduced state on the left hand side. n_O is calculated from difference in mass between a peak and the

following trough.

$$m_{peak} - m_{trough} = m_O \tag{2.2}$$

2.5 Scanning Electron Microscopy (SEM)

Scanning electron microscopy (SEM) works on the principle of of scanning the sample with a narrow electron beam while a detector measure the amount of electrons reflected back. This data for the lines scanned is then composited to a picture. Electron beams allow a smaller wavelength than visible light and thus a higher resolution. In addition as the electron beam hits the sample, the ground state electrons in an atom are excited and gets emitted. An electron from a higher energy shell then takes the emitted electrons place. The energy difference between these shells are emitted as characteristic X-rays which can be used to identify the elements on a certain point or map the element distribution of an entire surface. [22], [23], [24]

2.6 Chosen Materials And Their Applications

From Brorsson et al.'s list 1.1 four candidates were chosen for further study:

$$\tfrac{2}{3}\mathrm{CaO} + \tfrac{2}{3}\mathrm{CaCr_2O_4} + \mathrm{O_2} \rightleftharpoons \tfrac{4}{3}\mathrm{CaCrO_4} \qquad (1^{\mathrm{th}})$$

$$\mathrm{BaO} + 02 \rightleftharpoons 2\,\mathrm{BaO_2} \qquad (7^{\mathrm{th}})$$

$$\tfrac{2}{3}\mathrm{MgO} + \tfrac{2}{3}\mathrm{Cr_2MgO_4} + \mathrm{O_2} \rightleftharpoons \tfrac{4}{3}\mathrm{CrMgO_4} \qquad (9^{\mathrm{th}})$$

$$\tfrac{11}{9}\mathrm{AlLiO_2} + \tfrac{11}{9}\mathrm{CrLiO_2} + \mathrm{O_2} \rightleftharpoons \tfrac{1}{9}\mathrm{Al_{11}O_{18}} + \tfrac{11}{9}\mathrm{CrLi_2O_4} \qquad (19^{\mathrm{th}})$$

as well as the well studied Cuprous oxide–cupric oxide system for reference:

$$2\,\mathrm{Cu_2O} + \mathrm{O_2} \rightleftharpoons 4\mathrm{CuO}$$

These candidates will hereafter be referred to as "the calcium chromate system", "the barium oxide system", "the magnesium chromate system" and "the lithium based system".

2.6.1 Barium oxide

A barium oxide system has been proposed in many earlier studies for both TCES and as an OC [25], [26], [27] [28]. These studies has led to some promising results and the barium will be studied as a peer review.
Barium itself is a versatile metal with many varied applications and is used in many industries. A handful examples are as promoter in catalysts[29] for ammonia synthesis or as a catalyst in ethylbenzene oxidation to hydroperoxide[30], as a constituent in glass-ceramic materials[31], for semiconductors[32], sulphate precipitation[33] or as a stealth material in military applications [34]. Barium oxide itself has also been proposed for carbon capture and storage applications due to it´s reactivity with

CO2, quickly forming Barium Carbonate if not properly stored under a nitrogen atmosphere. [35]

2.6.2 Lithium aluminate

Lithium aluminate is commonly used for tritium breeding reactors, as a matrix in molten carbonate fuel cells, ceramic materials and as a lithium battery cathode material. [36],[37],[38],[39] To the authors knowledge no literature for the application of lithium aluminate in thermal energy storage has been proposed or studied with the exception of Brorrson's datamine approach.[13].

2.6.3 The Chemical Background of Chromium and its Dangers

Chromium appear among half the systems suggested by Brorsson's thermodynamical simulations in Table 1.1. A chromium based oxygen carrier hasn't been studied much in practice either. Typically, both chromium and aluminium oxides have a high stability, which would make them impractical for this application. Perhaps the inclusion of calcium, magnesium and lithium respectively, that on their own melt at low temperatures, could produce a functional system.

Cr(VI+) ions are known to be highly toxic and cancerogenic[40][41][42][43], which would be a downside of the Cr based systems if the chrome is in that oxidation state in any part of that system. If that is the case and such a system is found to have good technical properties, a discussion could be had about whether it could be sufficiently contained and if its technical performance is good enough to justify the hazards.

Calcium chromate has been used industrially as a corrosion inhibitor, strong oxidising agent, depolariser for batteries and as a coating for light metal alloys.[39] It is highly carcinogenic and toxic[44]. To the authors knowledge no literature for the application of calcium chromate in thermal energy storage has been proposed or studied with the exception of the datamined database. [12]

Lithium chromium oxide has been investigated as a possible cathode material for lithium ion batteries and as a material to be used in optical devices.[45] To the authors knowledge there have been no investigations into its use in TCES.

Magnesium Chromate has been utilised in different applications such as lightweight construction and corrosion resistance in the aerospace, electrical and automotive industries and as a promoter for paint adhesion. [46],[47] ,[48],[49]. To the authors knowledge no literature for the application of magnesium chromate in thermal energy storage has been proposed or studied with the exception of the datamined database. [12]

3

Method

This chapter details the methods and procedures used in this study to test the materials outlined in the theory, first synthesis and characterisation, the followed by TGA cycling. Table 3.1 summarises synthesis methods, reactants and calcination conditions for the samples produced.

Table 3.1: Overview of reactants and reaction conditions used during synthesis

Product	Reactants	Amount	Calcination temp. & time
	Sol-gel		
$MgO + Cr_2MgO_4$	$Mg(OH)_2$	14.3 mmol	800°C
	$Cr(NO_3)_3 \cdot 9\,H_2O$	14.3 mmol	16 h
	Citric acid monohydrate	24.33 mmol	
$CaO + CaCr_2O_4$	$Cr(NO_3)_3 \cdot 9\,H_2O$	8.45 mmol	1050°C
	$Ca(NO_3)_2 \cdot 4\,H_2O$	9.58 mmol	30 h
	Citric acid monohydrate	7.98 mmol	
$AlLiO_2$	$Al(OH)_3$	31,0 mmol	875°C
	$LiNO_3$	31.0 mmol	24 h
	Citric acid monohydrate	41.4 mmol	
$CrLiO_2$	$LiNO_3$	11.0 mmol	800°C
	$Cr(NO_3)_3 \cdot 9\,H_2O$	11.0 mmol	16 h
	Citric acid monohydrate	20.7 mmol	
	Solid state		
$MgO + Cr_2MgO_4$	Cr_2O_3	7.1 mmol	800°C
	MgO	28.4 mmol	16 h
$CaO + CaCr_2O_4$	Cr_2O_3	6.41 mmol	1050°C
	CaO	12.81 mmol	14 h
$AlLiO_2$	Al_2O_3	15.2 mmol	875°C
	Li_2CO_3	30.4 mmol	24 h
$CrLiO_2$	Cr_2O_3	10.11 mmol	850°C
	Li_2CO_3	20.19 mmol	16 h
BaO	$Ba(OH)_2$	29.17 mmol	750°C
	HNO_3	58.34 mmol	16 h

3.1 Synthesis

This part covers the sol-gel and solid state synthesis methods for the calcium chromate system, the barium oxide system, the magnesium chromate system and the lithium based systems. For the copper oxide reference system ready-made CuO was used.

3.1.1 The Magnesium Chromate System

The following section describes in short the methods used to synthesise and characterise the magnesium chromate system. Both the sol gel and solid state synthesis method was based on the article by K.R.[50].

Sol-Gel Synthesis
The target weight of the system (2 grams) was calculated for a molar ratio of 1:1 $Mg(OH)_2$ and $Cr(NO_3)_3$. 14.3 mmol of magnesium hydroxide and 14.3 mmol of chromium nitrate nonahydrate was dissolved in water and stirred with 24.33 mmol of citric acid monohydrate. The solution was left to evaporate at 98°C overnight. This resulted in a porous foamy deep purple blob that was crushed in an agate pestle. The powder was then put in a muffle furnace and calcinated at 800°C in air for 16 hours.

Solid State Synthesis
7.1 mmol of Cr_2O_3 and 28.4 mmol of MgO where weighed and mixed in a ball mill with no balls at 30 Hz for 30 min to obtain the 2:1 molar ratio of MgO and Cr_2MgO_4 of the final system. The sample was then calcinated in a muffle furnace at 1000°C for 16 hours with a 300°C/h ramp up and naturally cooled in the oven with no set ramp down.

3.1.2 The Calcium Chromate System

Sol-Gel Synthesis
8.45 mmol of $CrNO_3$, 9.58 mmol of $CaNO_3$ and 7.98 mmol of citric acid was dissolved in water and evaporated overnight. The gel was then calcinated at 1050°C for 30 h in a muffle furnace, with ramp up down of 300°C/h in air.

Solid State Synthesis
6.41 mmol of Cr_2O_3 and 12.81 mmol of CaO were mixed and ball milled for 30 min to reduce particle size. The powder mixture was then calcinated at 1050°C for 14 hours in a muffle furnace, with ramp up down of 300°C/h in air.

3.1.3 The Lithium Based System

The following section describes in short the methods used to synthesise and characterise the lithium based system. Both the sol-gel and solid state synthesis method of the $AlLiO_2$ was based on the articles written by Nguyen and Kinoshita [51, 52]. The synthesis method for $LiCrO_2$ was hard to find previous studies on and was therefore improvised without optimisation.

3.1.3.1 Sol-gel Synthesis

$AlLiO_2$
41.4 mmol of citric acid was dissolved in distilled water. 31.0 mmol of aluminium hydroxide was added and the mixture was stirred until a milky white that did not dissolve and was mixed with 31.o mmol of lithium nitrate that dissolved. The beaker was left stirring and evaporating on a hotplate and then dried overnight at 98°C resulting in a foamy yellow-tinted blob that was crushed with an agate pestle and mortar. It was then calcinated at 875°C for 24 hours.

$CrLiO_2$
20.7 mmol of citric acid was dissolved in distilled water. 11.0 mmol of $LiNO_3$ was added and dissolved. 11.0 mmol of $Cr(NO_3)_3$ nonahydrate aas added and dissolved. The solution was then evaporated and dried overnight at 98°C resulting in a puffy, porous, dark purple blob. It was ground with mortar and pestle. Put in a crucible and calcinated at 800°C in a muffle furnace in air atmosphere overnight.

3.1.3.2 Solid State Synthesis

$AlLiO_2$
15.2 mmol of Al_2O_3 and 30.4 mmol of Li_2CO_3 (a stoichiometric excess in order to account for its low vaporisation pressure) were mixed by ball mill for 30 minutes at 30 Hz with no balls. It was then calcinated at 875°C for 24 hours resulting in a very fine powder.

$CrLiO_2$
10.11 mmol of Cr_2O_3 and 20.19 mmol of $LiCO_3$ were ball milled for 40 min at 30 Hz. Calcinated overnight at 850°C for 16 h + ramp up/down of 300°C/h.

3.1.4 The Barium Oxide System

The following subsections describe the procedures done to synthesise and characterize barium oxide

3.1.4.1 XRD Results of $Ba(OH)_2$

The starting material that was available was barium hydroxide. The container was quite old and the nitrogen atmosphere required for storage had not been maintained.

The XRD showed that there was a mix of barium hydroxide, barium oxide and barium carbonate.

3.1.4.2 Nitration and Calcination of $Ba(OH)_2$

To solve the contamination problems and achieve barium oxide the barium was nitrated with 58.34 mmol HNO_3 at 68 percent concentration and then calcinated at 750°C for 16 hours to burn off the nitrates resulting in a melt that was pestled into a fine powder. After XRD and it being obvious from the yellow colour obtained from ocular inspection, there were still a mix of barium oxide and barium nitrate in the sample which was able to be burned off in the TGA. The sanple will hereby referred to as "barium oxide (nitration route)" In addition barium oxide was purchased from Sigma-Aldrich to test a pure quality controlled sample and will be referred to as "Barium oxide(purchased)".

3.2 PXRD

To confirm the identity of the samples, they were analysed with PXRD. This work was performed at the Chalmers Material Analysis Laboratory, CMAL. Utilising the Bruker D8 Discover instrument with a copper radiation source and low background holders. Measurements were taken at the angles given in Table 3.2. The data was then matched with reference spectrums in the Crystallography Open Database, COD, [53] using the software Bruker XRD Diffrac.EVA.

Table 3.2: Angles used for PXRD measurements

Compound(s)	Angles
$CaCrO_4$	10-65°
$Cr_2MgO_4 + MgO$	5-75°
$CrLiO_2$	15-75°
$AlLiO_2$	15-75°
BaO	5-55°

3.3 TGA

This section covers the programming and atmospheres used during the TGA experiments for all the systems. The experiments where run in "TGA Q500 V20.13 Build 39" located at the Divison of Energy and Materials on Chalmers university of technology. One of our aims are to determine the materials TCES capabilities. One of these are kinetics, but as explained in the theory section 2.4, for a full kinetics study to be done there is a requirement for different heating rates (ranging between 5-25°C/min) and multiple high quality reproducible data sets. Taking into account the limited access to the TGA instrument, it only being able to take one sample at a time (with manual changing of the sample), heating rates between 0-10°C/min and the amount of samples produced it is not possible to calculate the kinetics of the

reactions accurately within the scope of this study. In summary, there is a shortage of both time and the capabilities of the TGA equipment to perform a kinetic study to evaluate the suitability of the synthesised materials oxygen carrier applicability in TCES. The kinetics will only be determined by the rate of weight change, as the sample is oxidised or reduced, in comparison to the copper reference via ocular inspection.

3.3.1 Cupric Oxide Reference

Cupric oxide (CuO) is used as a reference to assure that our method works and there are no problems with the TGA itself. Once again the temperature limit of the TGA is a problem since its oxygen uncoupling behaviour starts at temperatures above 1050°C[54]. To get our reference the TGA was brought up to 1000°C at a ramping rate of 10°C/min and a gas flow of 90 ml/min. Synthetic air was switched to nitrogen at 1000°C changing the oxygen partial pressure from 0.21 to 0. This should cause the CuO to release it´s oxygen to become Cu2O causing the appropriate weight change.

3.3.2 The Magnesium Chromate System

Ramping rate was 10°C/min, constant flow of synthetic air at 90 ml/min. The sol-gel sample was first brought up to 300°C and kept isothermal for 90 minutes and then ramped up to 1000 and then kept at that temperature for 90 minutes with an additional cycle. The solid state was directly ramped to 1000°C being kept isothermal for 30 minutes, brought down to 300 and then back to 1000 for 30 minutes.

3.3.3 The Barium Oxide System

Ramping rate for Barium oxide (**nitration route**)was 10°C/min to 900°C, and then ramped down to 400 °C where the temperature was ramped in steps of 100 after a 15 minute isothermal interval with 1 repeated cycle. The atmosphere was a constant flow of synthetic air at 90 ml/min.

The **Purchased** barium oxide was ramped to 1000°C where the atmosphere was switched to nitrogen for 15 minutes. The sample was then ramped down to 400°C in air and then ramped up to 1000°C again with a swith to nitrogen for 15 minutes.

3.3.4 The Lithium Based System

Ramping rate was 10°C/min. The sol-gel sample was tested two times. The solid state system was not tested since solid state synthesised CrLiO2 was not achievable within the time constraints of this study
It was first ramped to 300 and then kept isothermal for 15 minutes and then ramped at 100°C with 15 minute isothermal intervals until 1000 degree Celsius which was then repeated once after the furnace cooled down to 300 Celsius at 10°C/min.

After the results were analysed the method above was then tested again between 300 and 700°C.

3.3.5 The Calcium Chromate System

The TGA was ramped to 1000°C at 10 C/min under nitrogen and then cycled with synthetic air at intervals of 90 minutes

3.4 SEM

Pictures and element point identification where done on a "Phenom ProX Desktop SEM" at 15kV, 1 Pa on a 100 µm scale. Due to time limitations EDX mapping of the samples couldn't be run.

4

Results and Discussion

This chapter details the results of the synthesis and TGA as referenced in the method section. For calculations regarding the degree of conversion see 2.4.1. The XRD results are summarised below with comments on the results and their synthesis in the corresponding subsection. The XRD spectrums are displayed in Appendix 1 XRD. This section details our TGA results which are summarised in Table 4.2. Since both barium oxide and calcium chromate changed form crystal powders into pellets after the TGA experiments. In addition the mass of the barium oxide sample increased between cycles from its starting mass. These effects could be dependent on effects such as agglomeration, crystal grain growth or changes in crystal structure. For this reason the powders were compared before and after TGA in SEM at (15 kV, 1 Pa) on a 100 µm scale Due to time limitations an EDX scan could not be run and settled for point element identifications. These results are summarised in Tables 4.1 and 4.2 on the page below

Table 4.1: Overview of the synthesis results from XRD analysis

Compound(s)	Sol-gel	Solid state
$CaCrO_4$	Success	Success
$Cr_2MgO_4 + MgO$	Success	Success
$CrLiO_2$	Success	Failed
$AlLiO_2$	Success	Failed
Compound	Nitration	Bought
BaO	Failed	Success

Table 4.2: Overview of TGA results

Sample	Temperature range (°C)	Atmosphere	Mass (mg)	Cycles	Degree of conversion
CuO	1000	Air, N2	37.56	1	100%
Sol-gel					
CaO + CaCr2O4	1000	Air, N2	25.55	5	36%
MgO+Cr2MgO4	400-1000	Air, N2	10.64	2	2%
AlLiO2 + CrLiO2	300-1000	Air	10.81	N/A	N/A
	300-700	Air	13.09	N/A	N/A
Solid state					
CaO + CaCr2O4	1000	Air, N2	17.31	5	55%
MgO + Cr2MgO4	400-1000	Air, N2	17.36	2	1%
BaO (nitration)	400-900	Air	39.96	2	N/A
BaO (purchased)	400-1000	Air, N2	21.48	2	N/A

4.1 Cupric Oxide Reference

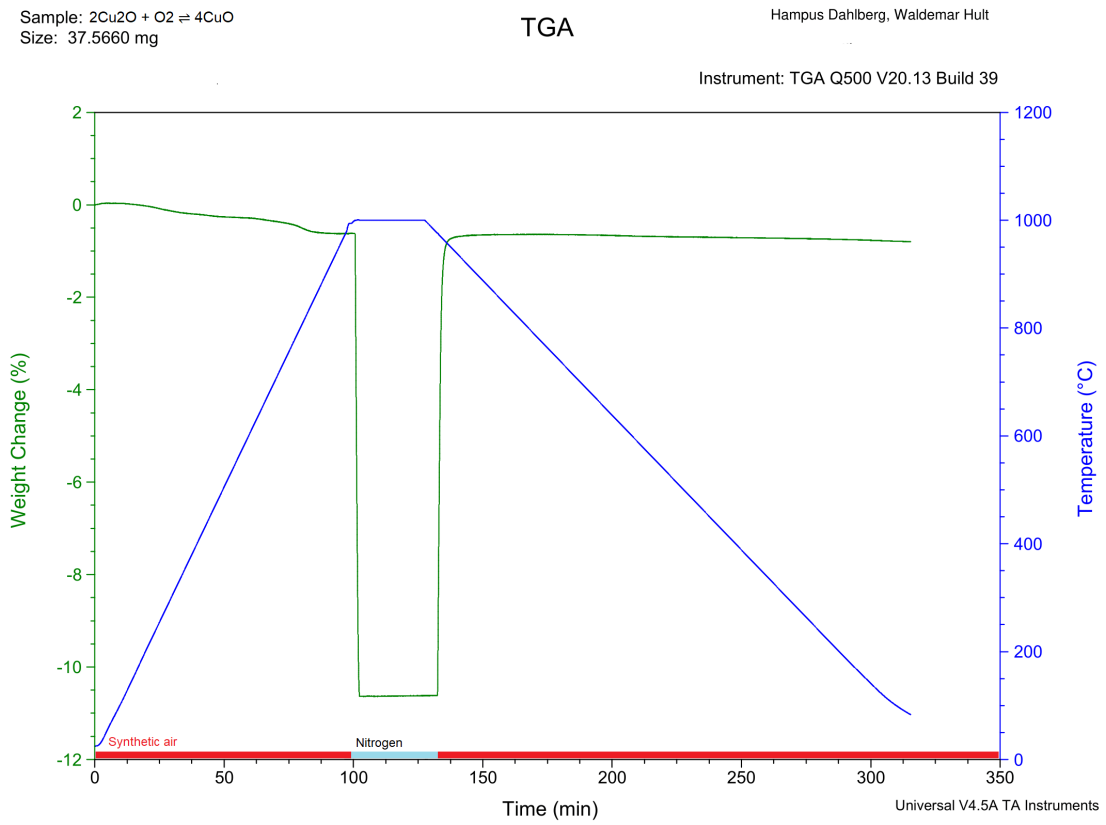

Figure 4.1: TGA curve for cupric oxide with nitrogen switch

The cuprous oxide works as described in the reference[54], and confirms that the nitrogen atmosphere method works as laid out in the method section 3.3.1 and is further confirmed by ocular inspection off Figure 4.1 and yields a 100% degree of conversion. One thing to note is that the mass change according to Mattiason et al. [54] in theory should be 9% and our reference sample exceeds that.

4.2 The Lithium Based System

4.2.1 Synthesis

The **solid state synthesis** of $AlLiO_2$ failed. No lithium was detected in the XRD spectrum and the lithium most probably evaporated during synthesis and was not pursued further because of problems with the corresponding $CrLiO_4$ synthesis.

The attempt to synthesise $CrLiO_2$ via solid state synthesis failed, and was not pursued further since the colouring of the crucible indicated physical vapor deposition of the desired product mixed with CrO_3 which is hazardous. See Figure 4.2.

(a) Inside of crucible after $CrLiO_2$ solid state synthesis.

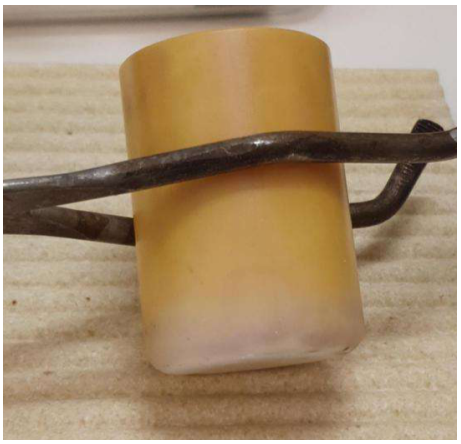

(b) Sideview of crucible after $CrLiO_2$ solid state synthesis. Original colour at the bottom

Figure 4.2: Crucible after $CrLiO_2$ solid state synthesis.

The **Sol-gel** synthesis of both $CrLiO_2$ and $AlLiO_2$ were successful without complications. The XRD analysis (See Figures A.8 and A.9 in Appendix A) showed a 0.5°phase shift which indicates either an impure phase or tensile strain/lattice expansion in the crystal structure.

4.2.2 TGA Cycling

As can be seen in both Figure 4.3 and 4.4 the system behaves like the other systems where any absorbed moisture is initially evaporated and the weight starts rising until around 600°C where the weight drops and the sample does nothing that is of interest for this study. In simple terms it deactivates and becomes inert for the purpose of an oxygen carrier particle. In addition after the TGA measurment the sample sintered into a loose pellet. In short the lithium based system doesn't fulfill the requirements of a TCES material.

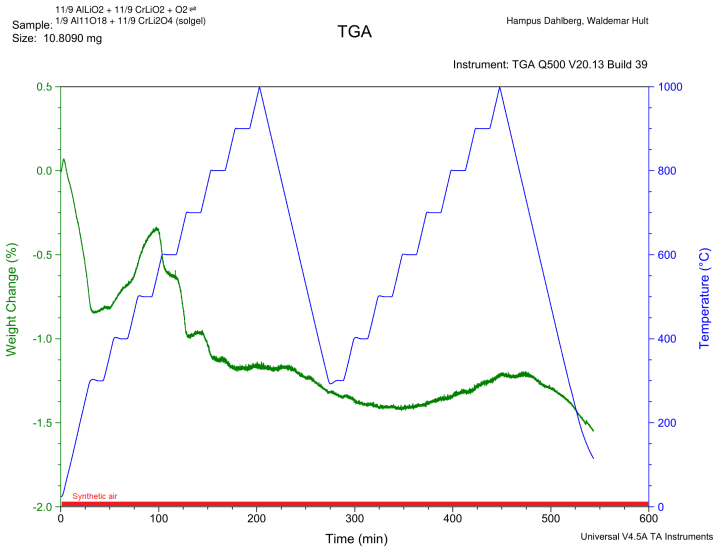

Figure 4.3: TGA curve for the lithium based system made by sol-gel synthesis between 300 and 1000 °C

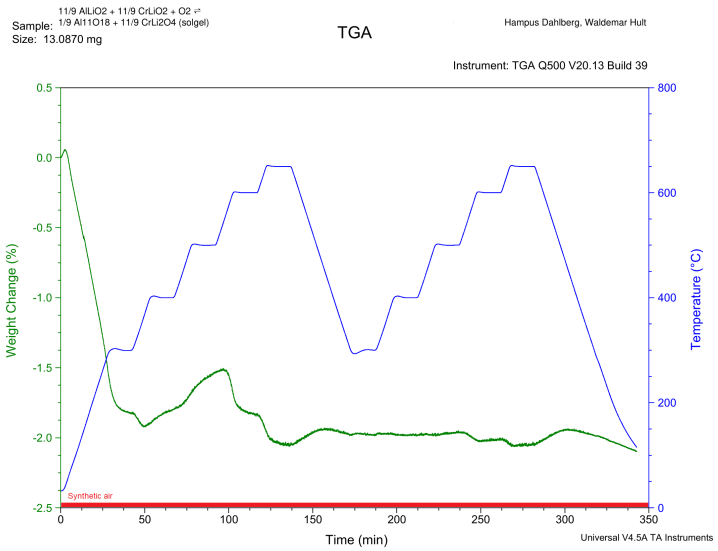

Figure 4.4: TGA curve for the lithium based system made by sol-gel synthesis between 300 and 700 °C

4.3 The Magnesium Chromate System

4.3.1 Synthesis

Cr_2MgO_4 was found in both samples. The solid state one was found to clearly contain MgO as well, as expected, but it was not clearly seen in the corresponding sol-gel spectrum. However it could be presumed to be present there as well because of the proportions Mg and Cr were added in, and its peaks closely match ones present in Cr_2MgO_4 which makes them harder to detect. Both methods of synthesis were problem free which makes the solid state synthesis method preferable since it has a much better atom economy.

4.3.2 TGA Cycling

Solid state
Initial weight change is adsorbed moisture from air leaving the sample. The weight change is so minimal that the noise from weight measurement is clearly displayed. The switch to nitrogen atmosphere in the second cycle paradoxically causes a weight increase in the sample, which can be seen in Figure 4.5, in addition the kinetics are extremely slow and is repeated in cycle 2 until the synthetic air tank ran out of gas. Assuming the proposed equation is happening the degree of conversion is 1%.

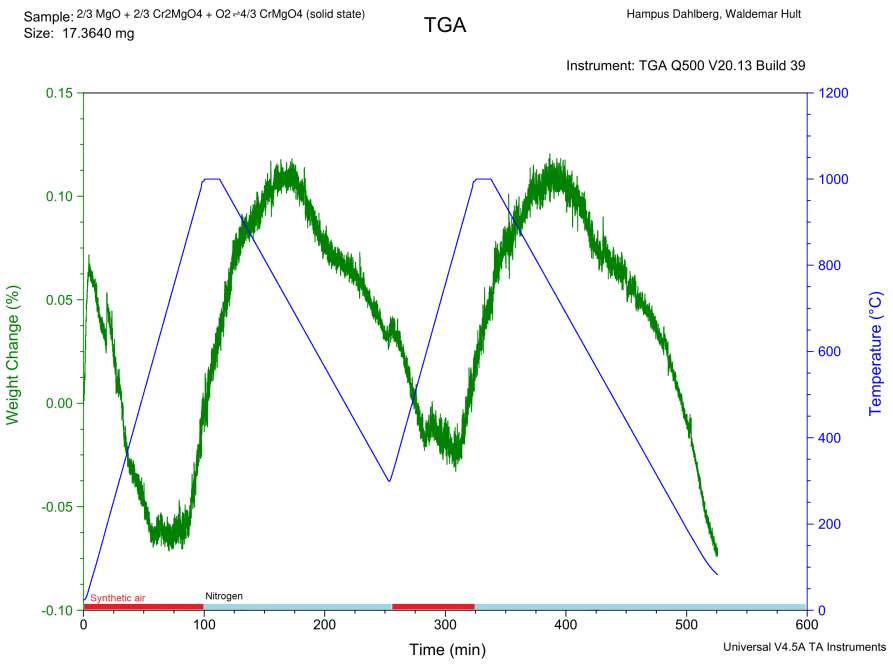

Figure 4.5: TGA curve for the magnesium chromate system made by solid state synthesis

Sol-gel
Initial weight change is adsorbed moisture from air leaving the sample. As can be seen in Figure 4.6 the sol-gel samples curve is identical to the solid state with the same paradoxical weight increase in a nitrogen atmosphere but it has a degree of conversion of 2% after 180 minutes. Since both samples are already in their reduced forms (See XRD results) there is a clear indication that the oxidation reaction requires higher temperatures than are available in the TGA furnace.

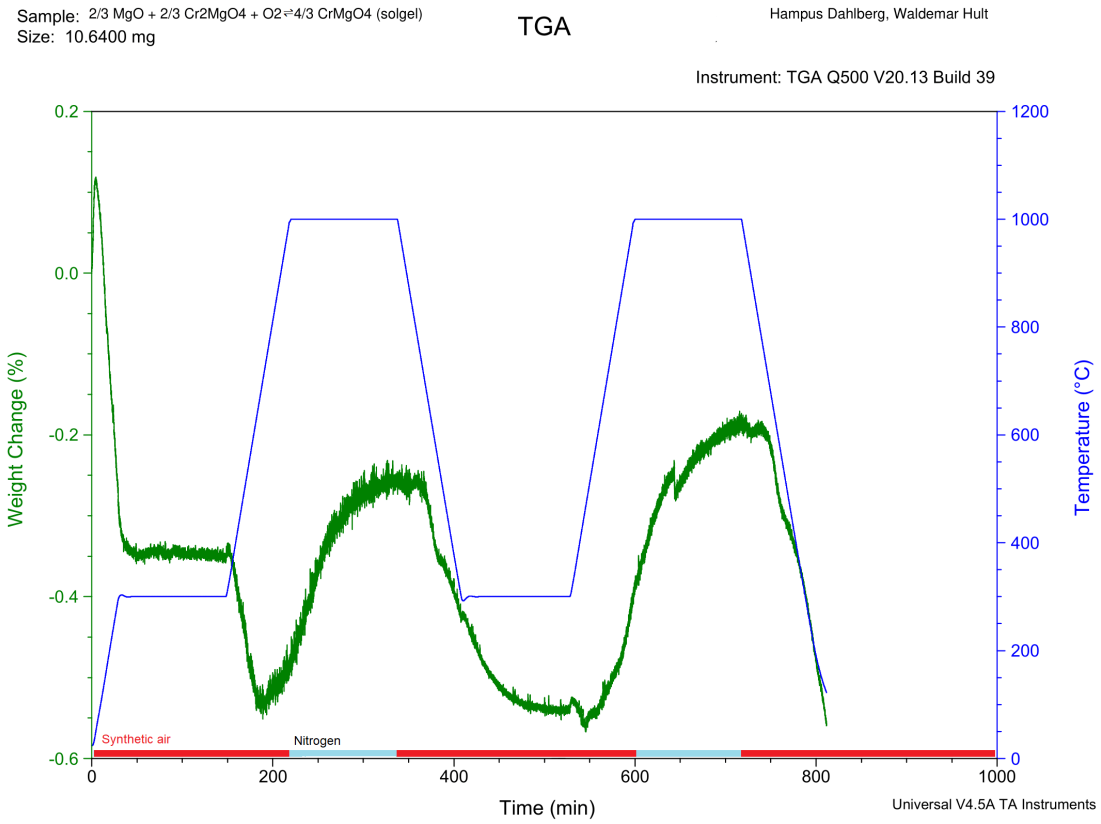

Figure 4.6: TGA curve for the magnesium chromate system made by sol-gel synthesis

4.3.3 Discussion

Both the **sol-gel** and **solid state** sample barely have a redox reaction at the set temperature and are slow to react. Even when the sol-gel samples have 3 hours to react, the weight only changes by 0.325% between the peaks. This conclusion is clearly evident by the low conversion yield and Figures 4.5 and 4.6.

A positive conclusion for the purpose of evaluation of Brorsson et al.'s article is that it is cycling and behave like an oxygen carrier particle candidate with poor performance.

4.4 The Barium Oxide System

4.4.1 Synthesis

The BaO made by nitrating and calcifying the impure barium hydroxide was found to still have remaining nitrates, but with major improvements. The purchased BaO was confirmed to be BaO.

4.4.2 TGA Cycling

Nitration route The TGA results in Figure A.1 starts as promising as the remaining nitrates are burned of at 1000°C and the sample takes up oxygen at lower temperatures with a drop over 800°C. But the weight keeps dropping and increasing further with each additional cycle. There is also an indication of multiple phases due to the multiple bumps which requires further investigation of Barium oxides crystalline behaviour and chemistry since no real conversion calculations would be relevant. It also melted into a brittle pellet that fused to the crucible which indicates thermal grain growth. An informal way to describe it would be a an elevation graph of hiking through hills.

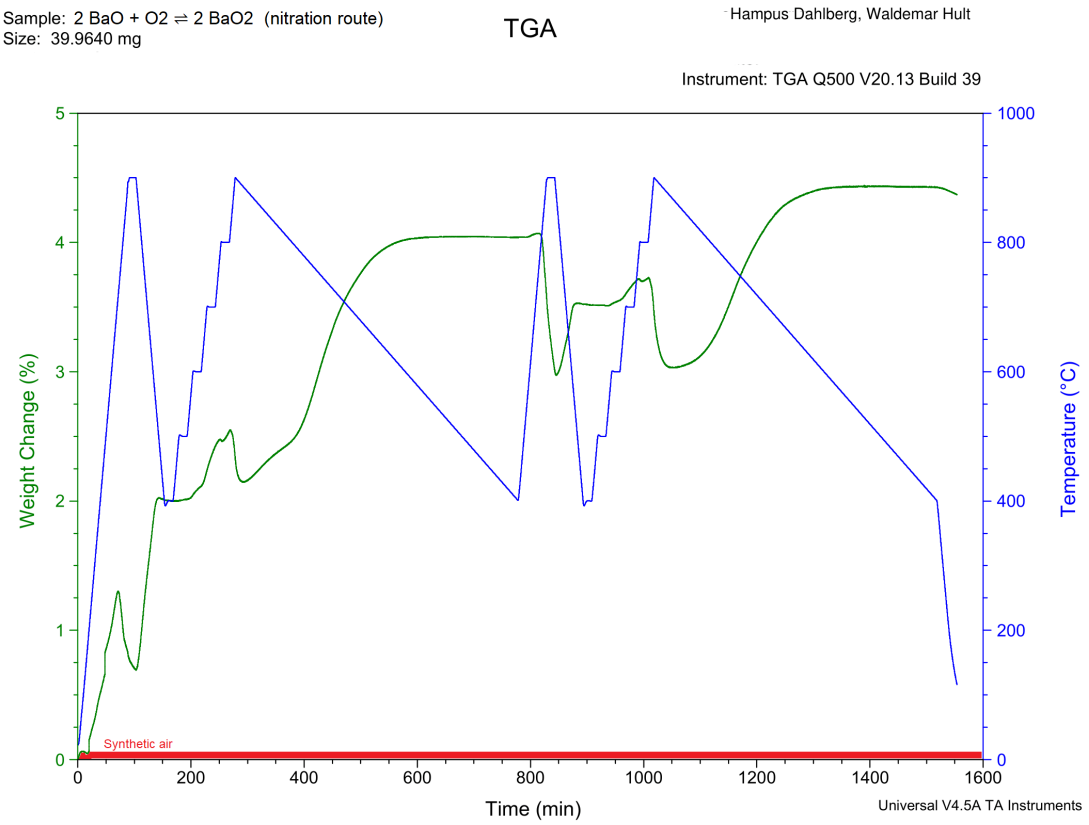

Figure 4.7: TGA curve for barium oxide made via the nitration route

Purchased BaO The Barium oxide bought from Sigma Aldrich behaves as an oxygen carrier in a cyclic manner but once again there is an indication of multiple phases due to the multiple bumps at 600 and 800°C in the first cycle, which repeats in the second cycle. The change in weight of the second cycle is also slightly lower. For both peaks with the swith to nitrogen atmosphere, we calculate the degree of conversion to be over 100%, further indicating that the real system is more complex than our theoretical one. The sample also melts into a hard pellet that fuses to the crucible.

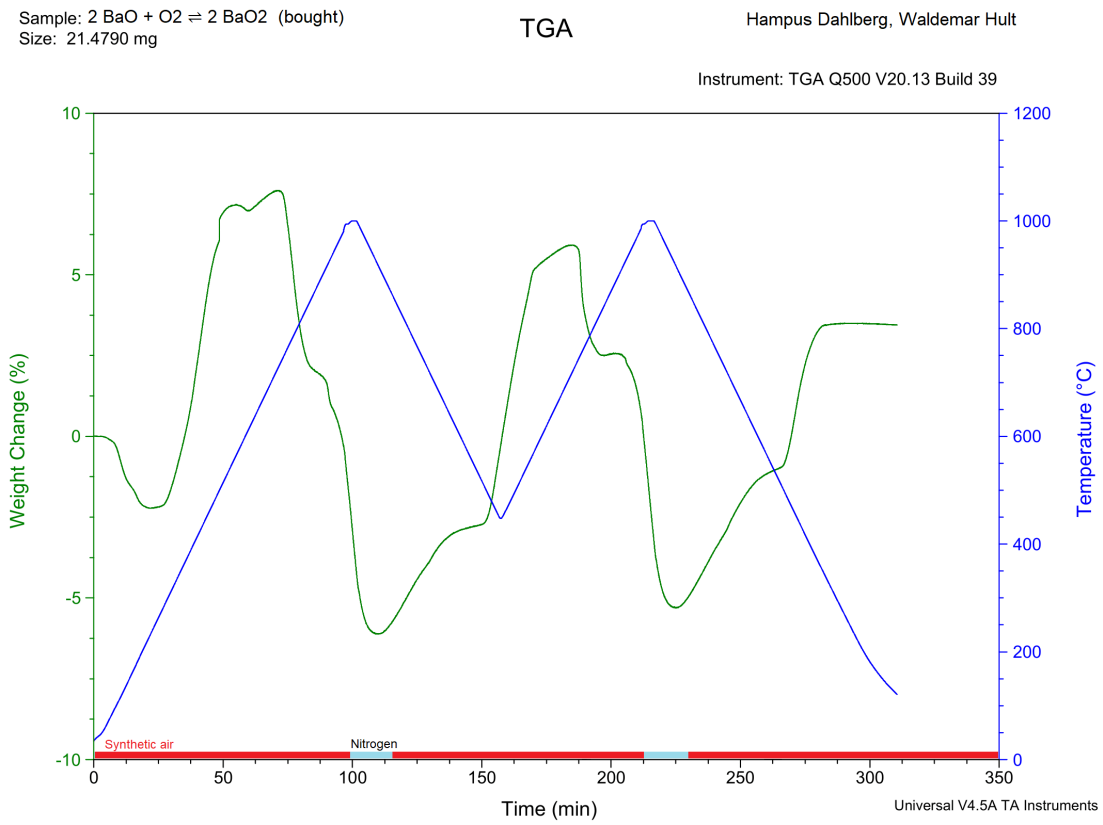

Figure 4.8: TGA curve for purchased barium oxide

4.4.3 SEM analysis

4.4.3.1 Nitration route

As can be seen in Figure 4.9a there are mainly small crystallites and few larger crystals not exceeding 20 µm in size. After the TGA measurements these have fused into dense networks where it can be observed in Figure 4.9b that they grow in a lamellar shape creating small tube-like pores that enclose upon further crystal grain growth, which explains the continuos rise in weight.

(a) BaO nitration route preTGA

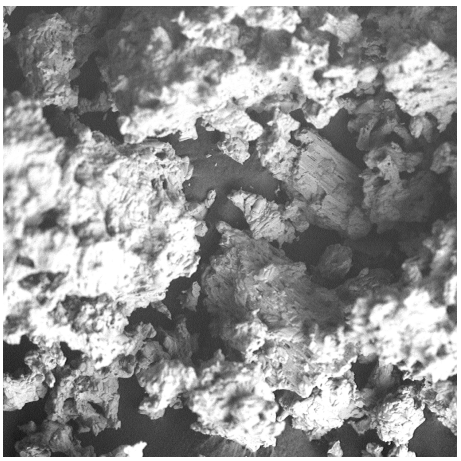

(b) BaO nitration route postTGA.

Figure 4.9: SEM pictures displaying changes in the BaO powder obtained from nitration purification before and after TGA measurement.

4.4.4 Purchased

As can be seen in Figure 4.10a there are a mix of rough particles and crystals in varying sizes which is expected from an industrial process. As can be seen in Figure 4.10b, after the TGA measurement these particles have transformed into quite large crystals with smooth surfaces. As can be more easily seen here, they still grow in a lamellar fashion which creates the enclosed pockets that causes the weight increase but also explains the lower efficiency in the second cycle as the sample has less surface area and explains the degree of conversion being over 100% as there is excess oxygen leaving the sample that is not bound to the metal.

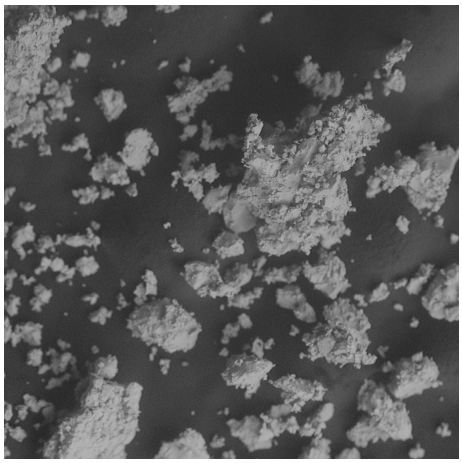

(a) BaO powder as purchased from Sigma-Aldrich.

(b) BaO powder purchased from Sigma-Aldrich after TGA

Figure 4.10: SEM pictures displaying changes in the BaO powder obtained from nitration purification before and after TGA measurement.

4.4.5 Discussion

Nitrated
As expected the small amount of remaining nitrates burned of, but the measurement is so inconsistent that no real discussion can be had other than that reduction takes place above 800°C and that the sample most probably does not have time to fully oxidise since the reaction requires lower temperatures. The fact that the powder melts and expands is also problematic. Due to limitation in time and access to the TGA a test (with improved method and nitrogen cycles) couldn't be performed.
Bought
The purchased barium oxide acts pretty close to the CuO reference, with a bit slower kinetics, in terms of conversion yield with the switch from air to nitrogen atmosphere. But with the powder agglomerating and fusing to the crucible even at lower temperatures its future for TCES needs improvements. The results are consistent with previously conducted research from Lei[25] and Carrillo[28]

4.5 The Calcium Chromate System

4.5.1 Synthesis

The sol-gel synthesis produced a $CaCrO_4$ XRD spectrum with clear peaks. The solid state synthesis resulted in a mix of $CaCrO_4$ and $CaCr_2O_4$, most probably due to the shorter synthesis time in the furnace. Both methods of synthesis were problem free but require long furnace times and are much easier to obtain through wet synthesis methods.

4.5.2 TGA Cycling

Solid state
As can be seen in Figure 4.11 there is a low increase in weight starting around 800°C and at 1000°C a significant and fast weight drop occurs. The solid state system consistently cycles at 5,5 weight percent throughout the measurement with a curve that matches the cuprous oxide reference (Figure 4.1) in appearance corresponding to a degree of conversion of 36% of the calcium chromate sample. But the sample doesn't fully re-oxidise to its original state evident by the 0,5 weight percent difference and the change in colour from lime green to an almost black green after completed analysis. The sample came out from the crucible as as a brittle foamy pellet, when crushed the original lime green colour returned with slight traces of black and the signature colour of Cr2O3.

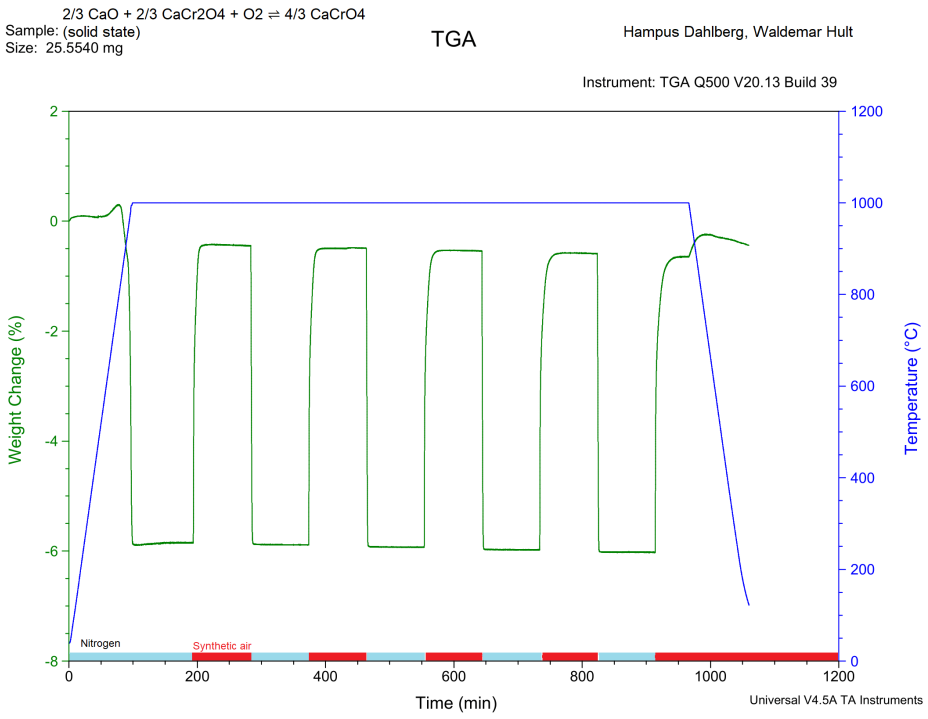

Figure 4.11: TGA curve for the calcium chromate system made by solid state synthesis

Sol-gel

As can be seen in Figure 4.12 there is a low increase in weight starting around 800°C and at 1000°C a significant and fast weight drop occurs which cycles at 8 percent throughout the measurement a curve that matches the cuprous oxide reference (Figure 4.1) in appearance with the difference of the last 1,5 weight percentage having a parabolic appearance corresponding to a degree of conversion of 55%. But the sample doesn't fully re-oxidise to its original state evident by the change in colour from lime green to an almost black green. The sample came out from the crucible as as a brittle foamy pellet. When crushed the original lime green colour returned with slight traces of black and the signature colour of Cr2O3.

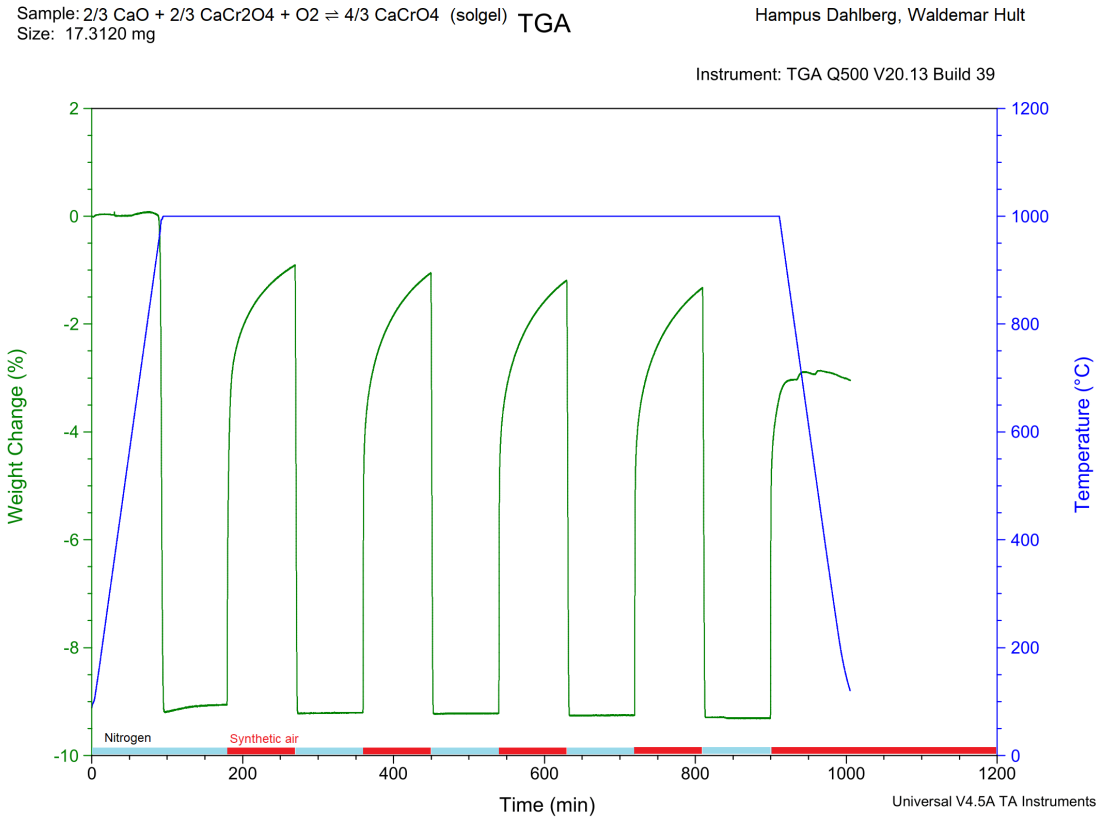

Figure 4.12: TGA curve for the calcium chromate system made by sol-gel synthesis

4.5.3 SEM Analysis

Solid state

As can be seen in Figure 4.13a before the TGA there where an abundance of mainly smaller crystals 5-25µm and larger ones in the size of 20 and few at the largest sizes in the 40-60 µm range. There are also two crystal structures that differ in appearance which is supported by the XRD results. As can be seen in Figure 4.13b ater the TGA measurment these have fused and agglomorated into porous interconnected networks with larger crystallites in the 40-100 µm range. Element point identification reveals mainly Calcium in the connective bridges and investigation of the 5 µm crystal grains from Figure 4.13c with vissualy different crystal structures reveals the presence of CaCrO4, CaCr2O4, CrO2 and Cr2O3. This confirms the assumption that the possible side reactions proposed by Brorsson in Table 1.1 is occurring

(a) CaCro4 solid state preTGA.

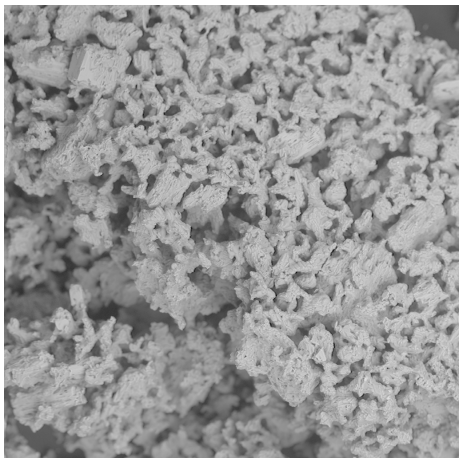

(b) CaCro4 solid state postTGA.

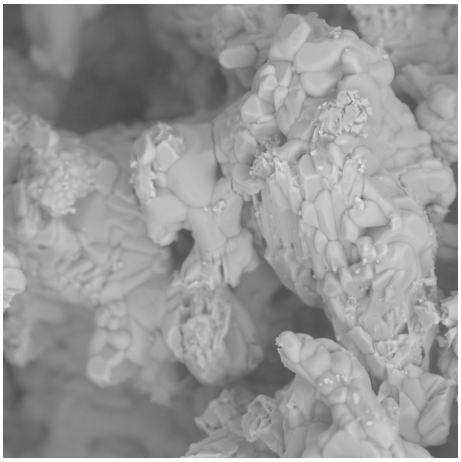

(c) CaCro4 solid state postTGA 30µm scale

Figure 4.13: SEM pictures displaying changes in the CaCrO4 solid state powder before and after TGA measurement in addition to 30 µm scale grain structure.

Sol-gel
As can be seen in Figure 4.14a before the TGA the main crystal sizes are in the range of 20-60 µm, in stark difference to the solid states many smaller crystals. As can be seen in Figure 4.14b. after the TGA measurment, these have fused and agglomorated into denser porous networks in comparison to the solid state sample and have smaller crystalites that are about 10-30 µ[]m. The same investigation of 5 µm crystal grains were performed, but we forgot to save the picture. The crystal grains were close to identical in appearance. Element point identification reveals calcium in the connective bridges and crystal grains with vissualy different crystal structures reveals the presence of CaCrO4, CaCr2O4, CrO2 and Cr2O3. Since CaO was in slight excess in the synthesis it is reasonable to assume that the excess is responsible for the denser agglomeration and parabolic curveshape of the TGA curve in Figure 4.12, which might have lead to the improved conversion yield.

(a) CaCro4 solgel preTGA.

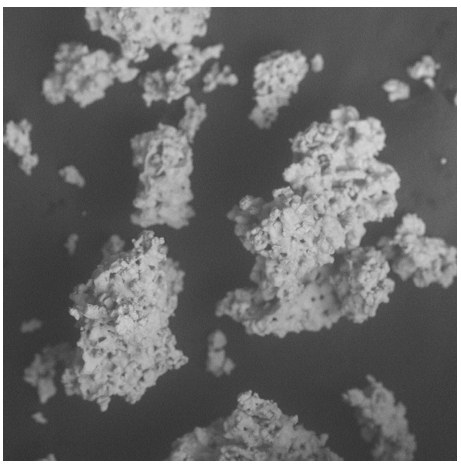

(b) CaCro4 solgel postTGA.

Figure 4.14: SEM pictures displaying changes in the CaCrO4 solgel powder before and after TGA measurement.

4.5.4 Discussion

In both cases the system is pretty much unresponsive until 1000°C but there is also a clear difference between the **sol-gel** and **Solid state** particles in redox behaviour where the solid state has the same kinetics in both reduction and oxidation while the sol-gel has a harder time to re-oxidise after it has uncoupled the oxygen. Both systems also agglomerated where smaller crystals melted and acted as solder between the bigger particles. There is also a slight rise in weight around 800 °C for both samples, being more noticeable in the solid state sample. The weight increase is strange because the temperature is ramping under a constant flow of nitrogen gas which indicates that the regular atmosphere is contaminating the TGA´s gas flow since the TGA furnace is open to the air.
Brorsson et al.'s list[13] suggests two side reactions in System 8 and 20 where the equilibrium temperature is lower than for System 1:

$$CaCr_2O_4 + O_2 \rightleftharpoons CrO_2 + CaCrO_4$$

$$\tfrac{4}{3}CaCr_2O_4 + O_2 \rightleftharpoons \tfrac{2}{3}Cr_2O_3 + \tfrac{4}{3}CaCrO_4$$

This is supported by the shifting weight curves at the end of both measurements, occurring below 750 degrees for the sol-gel sample and below 900 degrees for the solid state sample when the atmosphere switches to oxygen. Further proof for this hypothesis is the change in colour of the sample as Cr(+IV)O2 is black and Cr(+III) is green. This theory was confirmed through point element identification in SEM.
Aside from this both samples perform at the same level of quality as the cuprous oxide reference in terms of kinetics and has a competitive degree of conversion.

5
Conclusion

Since trivalent chromium based compounds are notorious for having very slow kinetics, the calcium chromate system would never have been a suggestion for oxygen carrier research based on the average chemist's intuition. Both $CaCr_2O_4$ and $CaCrO_4$ are rarely studied as is. So our results were unexpected. The material could be oxidized and reduced at 1000°C by cycling between air and inert atmosphere with a molar degree of conversion of 55% and 36% for material produced via sol-gel and solid state synthesis respectively. This suggests suitability as a TCES material.

Barium oxide works as an oxygen carrier but has problems with agglomeration and a need for proper storage and maintenance since it reacts with most organic solvents and carbon dioxide in air.

The magnesium chromate system works as described by the definition of TCES material but its kinetics are slow and would require very high temperatures. The performance is as expected given the usual stability of chromium based oxides.

The lithium aluminate system does not meet the requirements for a TCES material and the solid state synthesis of $CrLiO_2$ with lithium carbonate is dangerous.

Finding possible materials for TCES is challenging both in terms of finding good candidates for research and resources the research itself requires. Brorsson et al.'s proposal [13] for mining databases to find these candidates has been confirmed to provide both guidance and suggestions for materials that goes against intuition.

§

Bibliography

[1] Haisheng Chen, Thang Ngoc Cong, Wei Yang, Chunqing Tan, Yongliang Li, and Yulong Ding. Progress in electrical energy storage system: A critical review. *Progress in Natural Science*, 19(3):291–312, 3 2009. ISSN 1002-0071. doi: 10.1016/J.PNSC.2008.07.014.

[2] I. Cañadas, D. Martínez, and J. Rodríguez. Materials thermal treatment at plataforma Solar de Almeria Solar Furnace: Current activity lines. In *Boletin de la Sociedad Espanola de Ceramica y Vidrio*, volume 43, pages 591–595. Sociedad Espanola de Ceramica y Vidrio, 2004. doi: 10.3989/cyv.2004.v43.i2.602.

[3] Yunshu Zhang, Ye Cai, Sung Hwan Hwang, Gregory Wilk, Freddy DeAngelis, Asegun Henry, and Kenneth H. Sandhage. Containment materials for liquid tin at 1350°C as a heat transfer fluid for high temperature concentrated solar power. *Solar Energy*, 164:47–57, 4 2018. ISSN 0038-092X. doi: 10.1016/J.SOLENER.2018.01.085. URL `https://www.sciencedirect.com/science/article/pii/S0038092X18301063`.

[4] Md Parvez Islam and Tetsuo Morimoto. Advances in low to medium temperature non-concentrating solar thermal technology. *Renewable and Sustainable Energy Reviews*, 82:2066–2093, 2 2018. ISSN 1364-0321. doi: 10.1016/J.RSER.2017.08.030. URL `https://www.sciencedirect.com/science/article/pii/S1364032117311772`.

[5] Tawfiq Chekifi and Moustafa Boukraa. CFD applications for sensible heat storage: A comprehensive review of numerical studies. *Journal of Energy Storage*, 68, 9 2023. ISSN 2352152X. doi: 10.1016/j.est.2023.107893.

[6] Adrián Caraballo, Santos Galán-Casado, Ángel Caballero, and Sara Serena. Molten salts for sensible thermal energy storage: A review and an energy performance analysis, 2 2021. ISSN 19961073.

[7] Bhartendu Mani Tripathi, Shailendra Kumar Shukla, and Pushpendra Kumar Singh Rathore. A comprehensive review on solar to thermal energy conversion and storage using phase change materials. *Journal of Energy Storage*, 72:108280, 11 2023. ISSN 2352-152X. doi: 10.1016/J.EST.2023.108280. URL `https://www.sciencedirect.com/science/article/pii/S2352152X23016778`.

[8] Duygu Yilmaz, Esraa Darwish, and Henrik Leion. Investigation of the combined Mn-Si oxide system for thermochemical energy storage applications. *Journal of Energy Storage*, 28, 4 2020. ISSN 2352152X. doi: 10.1016/j.est.2019.101180.

[9] Inaki Adanez-Rubio, Alberto Abad, Henrik Leion, Tobias Mattisson, and Juan Adanez. Interaction of Swine Manure Ash-Oxygen Carrier Particles

under Chemical Looping Conditions. *Energy and Fuels*, 2 2025. ISSN 15205029. doi: 10.1021/acs.energyfuels.4c05071.

[10] Gajanan Dattarao Surywanshi, Henrik Leion, and Amir H. Soleimanisalim. Environmental impacts of a chemical looping combustion plant with a negative emission using bark as a feedstock. *Journal of Environmental Chemical Engineering*, 13(2):116040, 4 2025. ISSN 2213-3437. doi: 10.1016/J.JECE.2025.116040. URL `https://www.sciencedirect.com/science/article/pii/S2213343725007365?via%3Dihub`.

[11] Yongliang Yan, Ke Wang, Peter T. Clough, and Edward J. Anthony. Developments in calcium/chemical looping and metal oxide redox cycles for high-temperature thermochemical energy storage: A review. *Fuel Processing Technology*, 199:106280, 3 2020. ISSN 0378-3820. doi: 10.1016/J.FUPROC.2019.106280.

[12] Joakim Brorsson, Viktor Rehnberg, Adam A. Arvidsson, Henrik Leion, Tobias Mattisson, and Anders Hellman. Discovery of Oxygen Carriers by Mining a First-Principle Database. *Journal of Physical Chemistry C*, 127(20): 9437–9451, 5 2023. ISSN 19327455. doi: 10.1021/acs.jpcc.2c08545.

[13] Joakim Brorsson, Henrik Leion, and Anders Hellman. Discovery of thermochemical energy storage materials via a hy-brid data-mining approach. Technical report.

[14] V. Grover, Balaji P. Mandal, and A. K. Tyagi. Solid State Synthesis of Materials. In *Handbook on Synthesis Strategies for Advanced Materials Volume-I: Techniques and Fundamentals*, chapter 1, pages 1–49. Springer Nature Singapore Pte Ltd, Mumbai, India, 2021. doi: 10.1007/978-981-16-1807-9{_}1.

[15] Sana Elbashir, Markus Broström, and Nils Skoglund. Thermodynamic modelling assisted three-stage solid state synthesis of high purity β-Ca3(PO4)2. *Materials and Design*, 238, 2 2024. ISSN 18734197. doi: 10.1016/j.matdes.2024.112679.

[16] Calvin Nyarangi, Phani Ravi Teja Nunna, Nidal Abu-Zahra, Nadeem Baig, Ismail Abdulazeez, and Isam H. Aljundi. Optimizing the synthesis process for Lithium-Ion sieve adsorbents: Effect of calcination temperature and heating rate on reaction efficiency and performance. *Materials and Design*, 235, 11 2023. ISSN 18734197. doi: 10.1016/j.matdes.2023.112417.

[17] Scott D. Thiel, Alexandra D. Tamerius, and James P.S. Walsh. X-ray diffraction methods for high-pressure solid-state synthesis. In *Comprehensive Inorganic Chemistry III*, pages 200–221. Elsevier, 2023. doi: 10.1016/B978-0-12-823144-9.00103-5.

[18] Ashleigh E. Danks, Simon R. Hall, and Zoe Schnepp. The evolution of 'sol-gel' chemistry as a technique for materials synthesis. *Materials Horizons*, 3(2):91–112, 3 2016. ISSN 20516355. doi: 10.1039/c5mh00260e.

[19] Andrei A. Bunaciu, Elena gabriela Udriştioiu, and Hassan Y. Aboul-Enein. X-Ray Diffraction: Instrumentation and Applications, 10 2015. ISSN 15476510.

[20] A. W. Coats and J. P. Redfern. Thermogravimetric analysis. A review. *The Analyst*, 88(1053):906–924, 1963. ISSN 00032654. doi: 10.1039/AN9638800906.

[21] Sergey Vyazovkin, Alan K. Burnham, José M. Criado, Luis A. Pérez-Maqueda, Crisan Popescu, and Nicolas Sbirrazzuoli. ICTAC Kinetics Committee recommendations for performing kinetic computations on thermal analysis data. *Thermochimica Acta*, 520(1-2):1–19, 6 2011. ISSN 0040-6031. doi: 10.1016/J.TCA.2011.03.034.

[22] A. M. Paredes. MICROSCOPY | Scanning Electron Microscopy. *Encyclopedia of Food Microbiology: Second Edition*, pages 693–701, 1 2014. doi: 10.1016/B978-0-12-384730-0.00215-9. URL `https://www.sciencedirect.com/science/article/abs/pii/B9780123847300002159?via%3Dihub`.

[23] Yanet Rodríguez Herrero, Karen Lopez Camas, and Aman Ullah. Characterization of biobased materials. *Advanced Applications of Biobased Materials: Food, Biomedical, and Environmental Applications*, pages 111–143, 1 2023. doi: 10.1016/B978-0-323-91677-6.00005-2. URL `https://www.sciencedirect.com/science/article/abs/pii/B9780323916776000052`.

[24] J. Webb and J.H. Holgate. MICROSCOPY | Scanning Electron Microscopy. *Encyclopedia of Food Sciences and Nutrition*, pages 3922–3928, 1 2003. doi: 10.1016/B0-12-227055-X/00779-3. URL `https://www.sciencedirect.com/science/article/abs/pii/B012227055X007793`.

[25] Fuqiong Lei, Alexander Dyall, and Nick AuYeung. An in-depth investigation of BaO2/BaO redox oxides for reversible solar thermochemical energy storage. *Solar Energy Materials and Solar Cells*, 223:110957, 5 2021. ISSN 0927-0248. doi: 10.1016/J.SOLMAT.2021.110957.

[26] R G Bowrey and J Jutsen. Energy storage using the reversible oxidation of barium oxide. Technical report, Department of Chemical Engineering, University of New South Wales, 1978.

[27] Syed Saqline, Haiming Wang, Qianwenhao Fan, Felix Donat, Christoph Müller, and Wen Liu. Investigation of barium iron oxides for CO2 capture and chemical looping oxygen uncoupling. *Applications in Energy and Combustion Science*, 17:100238, 3 2024. ISSN 2666-352X. doi: 10.1016/J.JAECS.2023.100238.

[28] A. J. Carrillo, D. Sastre, D. P. Serrano, P. Pizarro, and J. M. Coronado. Revisiting the BaO2/BaO redox cycle for solar thermochemical energy storage. *Physical Chemistry Chemical Physics*, 18(11):8039–8048, 3 2016. ISSN 14639076. doi: 10.1039/c5cp07777j.

[29] Yeqin Guan, Weijin Zhang, Qianru Wang, Claudia Weidenthaler, Anan Wu,

Wenbo Gao, Qijun Pei, Hanxue Yan, Jirong Cui, Han Wu, Sheng Feng, Runze Wang, Hujun Cao, Xiaohua Ju, Lin Liu, Teng He, Jianping Guo, and Ping Chen. Barium chromium nitride-hydride for ammonia synthesis. *Chem Catalysis*, 1(5):1042–1054, 10 2021. ISSN 2667-1093. doi: 10.1016/J.CHECAT.2021.08.006.

[30] P. P. Toribio, J. M. Campos-Martin, and J. L.G. Fierro. Liquid-phase ethylbenzene oxidation to hydroperoxide with barium catalysts. *Journal of Molecular Catalysis A: Chemical*, 227(1-2):101–105, 3 2005. ISSN 1381-1169. doi: 10.1016/J.MOLCATA.2004.10.003.

[31] Janusz Partyka. Effect of BaO ratio on the structure of glass–ceramic composite materials from the SiO2–Al2O3–Na2O–K2O–CaO system. *Ceramics International*, 41(8):9337–9343, 9 2015. ISSN 0272-8842. doi: 10.1016/J.CERAMINT.2015.03.282.

[32] N. Abbas, J. M. Zhang, S. Nazir, H. Akhtar, M. Zaqa, S. Saleem, and G. Mustafa. Synthesis and characterization of Fe-substituting BaO nanoparticles by sol-gel method. *Digest Journal of Nanomaterials and Biostructures*, 18(4):1327–1338, 10 2023. ISSN 18423582. doi: 10.15251/DJNB.2023.184.1327.

[33] P. S. Hlabela, H. W.J.P. Neomagus, F. B. Waanders, and O. S.L. Bruinsma. Thermal reduction of barium sulphate with carbon monoxide—A thermogravimetric study. *Thermochimica Acta*, 498(1-2):67–70, 1 2010. ISSN 0040-6031. doi: 10.1016/J.TCA.2009.10.004.

[34] Ming Wu, Wenjie Dong, Luoguo Wang, Weizhao Yao, and Kai Li. Preparation and characterization of barium ferrite by self-propagating method. In Lvqing Yang, editor, *Seventh International Conference on Advanced Electronic Materials, Computers, and Software Engineering (AEMCSE 2024)*, volume 13229, page 1322907. SPIE, 2024. doi: 10.1117/12.3038171. URL `https://doi.org/10.1117/12.3038171`.

[35] Ryo Inoue, Shigeru Ueda, Koji Wakuta, Kohei Sasaki, and Tatsuro Ariyama. Thermodynamic consideration on the absorption properties of carbon dioxide to basic oxide. *ISIJ International*, 50(11):1532–1538, 2010. ISSN 09151559. doi: 10.2355/isijinternational.50.1532.

[36] Su Jeong Heo, Boxun Hu, Venkata Manthina, Abdelkader Hilmi, Chao Yi Yuh, Arun Surendranath, and Prabhakar Singh. Stability of lithium aluminate in reducing and oxidizing atmospheres at 700 °C. *International Journal of Hydrogen Energy*, 41(41):18884–18892, 11 2016. ISSN 0360-3199. doi: 10.1016/J.IJHYDENE.2016.03.145.

[37] Nagesh Ghuge, Debapriya Mandal, Mulrajsinh Jadeja, and Bahubali Chougule. Thermo-gravimetric kinetics analysis for the synthesis of lithium aluminate and fabrication of pebbles by solid state reaction process. *Journal of the Indian Chemical Society*, 99(4):100412, 4 2022. ISSN 0019-4522. doi: 10.1016/J.JICS.2022.100412.

[38] Sebastian Simon, Marko Bertmer, and Gregor J.G. Gluth. Sol–gel synthesis and characterization of lithium aluminate (L–A–H) and lithium aluminosilicate (L–A–S–H) gels. *International Journal of Applied Ceramic Technology*, 19(6):3179–3190, 11 2022. ISSN 17447402. doi: 10.1111/ijac.14187.

[39] Michael D. Larrañaga, Richard J. Lewis, and Robert A. Lewis. *Hawley's Condensed Chemical Dictionary, Sixteenth Edition*. Wiley, sixteenth edition edition, 9 2016. ISBN 9781118135150. doi: 10.1002/9781119312468.

[40] Max Costa. Toxicity and Carcinogenicity of Cr(VI) in Animal Models and Humans. *Critical Reviews in Toxicology*, 27(5):431–442, 1997. doi: 10.3109/10408449709078442. URL `https://doi.org/10.3109/10408449709078442`.

[41] Thomas Liborio DesMarias and Max Costa. Mechanisms of chromium-induced toxicity. *Current Opinion in Toxicology*, 14:1–7, 4 2019. ISSN 2468-2020. doi: 10.1016/J.COTOX.2019.05.003. URL `https://www.sciencedirect.com/science/article/pii/S2468202019300294`.

[42] Debasis Bagchi, Sidney J. Stohs, Bernard W. Downs, Manashi Bagchi, and Harry G. Preuss. Cytotoxicity and oxidative mechanisms of different forms of chromium. *Toxicology*, 180(1):5–22, 10 2002. ISSN 0300-483X. doi: 10.1016/S0300-483X(02)00378-5. URL `https://www.sciencedirect.com/science/article/pii/S0300483X02003785`.

[43] Xiaoyan Zheng, Siyu Li, Jiayi Li, Yueying Lv, Xiaoqiao Wang, Pengfei Wu, Qingyue Yang, Yuqing Tang, Yan Liu, and Zhigang Zhang. Hexavalent chromium induces renal apoptosis and autophagy via disordering the balance of mitochondrial dynamics in rats. *Ecotoxicology and Environmental Safety*, 204:111061, 11 2020. ISSN 0147-6513. doi: 10.1016/J.ECOENV.2020.111061. URL `https://www.sciencedirect.com/science/article/pii/S0147651320309003`.

[44] F J C Roe and R L Carter. CHROMIUM CARCINOGENESIS: CALCIUM CHROMATE AS A POTENT CARCINOGEN FOR THE SUBCUTANEOUS TISSUES OF THE RAT. Technical report, Chester Beatty Research Institute, London, 10 1968.

[45] H. I. Elsaeedy. Synthesis and Characterization of LiCrO2 Thin Films As Potential Cathode Material for Lithium Ion Batteries. *Journal of Electronic Materials*, 49(1):282–289, 1 2020. ISSN 1543186X. doi: 10.1007/s11664-019-07787-2.

[46] P. Sahoo, S. K. Das, and J. Paulo Davim. Surface Finish Coatings. *Comprehensive Materials Finishing*, 3-3:38–55, 2017. doi: 10.1016/B978-0-12-803581-8.09167-0.

[47] J. E. Gray and B. Luan. Protective coatings on magnesium and its alloys — a critical review. *Journal of Alloys and Compounds*, 336(1-2):88–113, 4 2002. ISSN 0925-8388. doi: 10.1016/S0925-8388(01)01899-0.

[48] Gaurang Bhargava and Fred Allen. Self-Healing, Chromate-free Conversion Coating for Magnesium Alloys. *Metal Finishing*, 110(4):32–38, 5 2012. ISSN 0026-0576. doi: 10.1016/S0026-0576(13)70127-2.

[49] Mustafa Kemal Kulekci. Magnesium and its alloys applications in automotive industry. *International Journal of Advanced Manufacturing Technology*, 39 (9-10):851–865, 11 2008. ISSN 02683768. doi: 10.1007/s00170-007-1279-2.

[50] K. Rida, A. Benabbas, F. Bouremmad, M. A. Peña, and A. Martínez-Arias. Influence of the synthesis method on structural properties and catalytic activity for oxidation of CO and C3H6 of pirochromite MgCr2O4. *Applied Catalysis A: General*, 375(1):101–106, 2 2010. ISSN 0926-860X. doi: 10.1016/J.APCATA.2009.12.024.

[51] Nguyen Thi Thu Ha, Trinh Van Giap, and Nguyen Trong Thanh. Synthesis of lithium aluminate for application in radiation dosimetry. *Materials Letters*, 267:127506, 5 2020. ISSN 0167-577X. doi: 10.1016/J.MATLET.2020.127506.

[52] K. Kinoshita, J. W. Sim, and G. H. Kucera. Synthesis of fine particle size lithium aluminate for application in molten carbonate fuel cells. *Materials Research Bulletin*, 14(10):1357–1368, 10 1979. ISSN 0025-5408. doi: 10.1016/0025-5408(79)90016-3.

[53] Saulius Gražulis, Daniel Chateigner, Robert T Downs, A F T Yokochi, Miguel Quirós, Luca Lutterotti, Elena Manakova, Justas Butkus, Peter Moeck, and Armel Le Bail. Crystallography Open Database – an open-access collection of crystal structures. *Journal of Applied Crystallography*, 42(4):726–729, 8 2009. doi: 10.1107/S0021889809016690. URL `https://doi.org/10.1107/S0021889809016690`.

[54] Tobias Mattisson, Anders Lyngfelt, and Henrik Leion. Chemical-looping with oxygen uncoupling for combustion of solid fuels. *International Journal of Greenhouse Gas Control*, 3(1):11–19, 2009. ISSN 17505836. doi: 10.1016/j.ijggc.2008.06.002.

A

Appendix 1 XRD

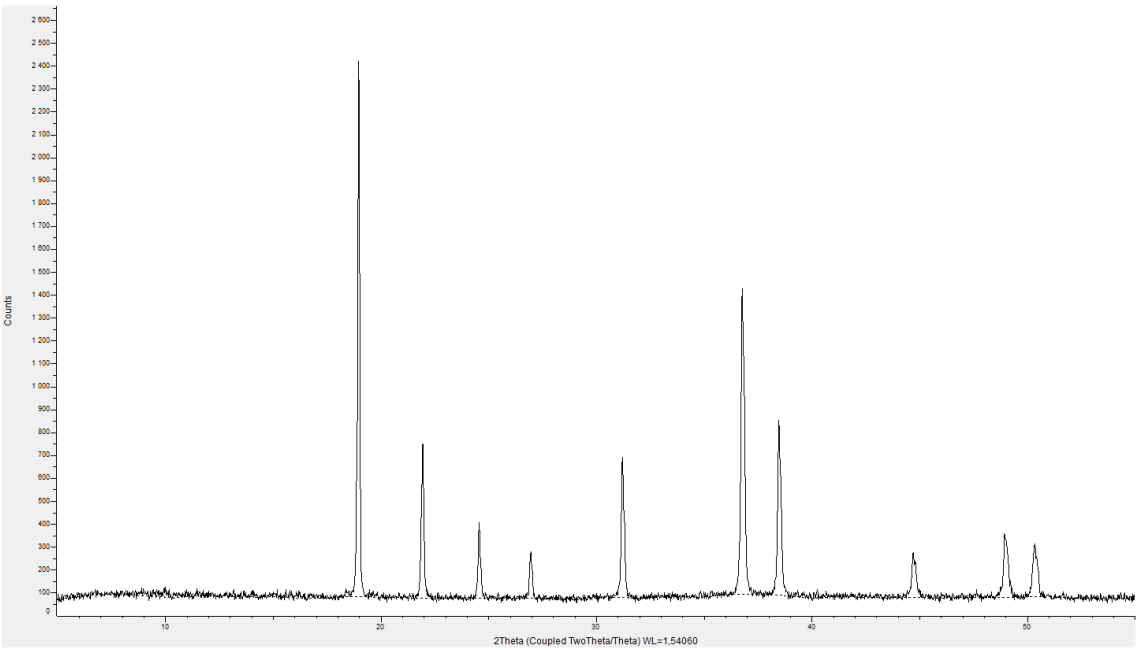

Figure A.1: XRD spectrum of BaO made through the nitration route

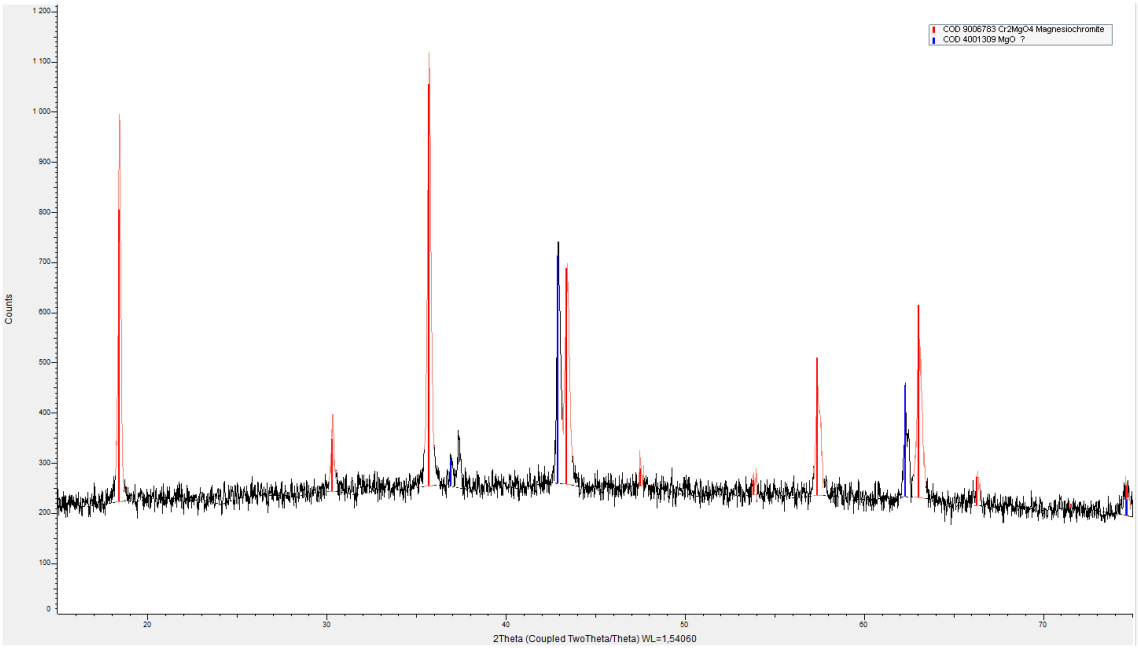

Figure A.2: XRD spectrum of $Cr_2MgO_4 + MgO$ made by solid state synthesis

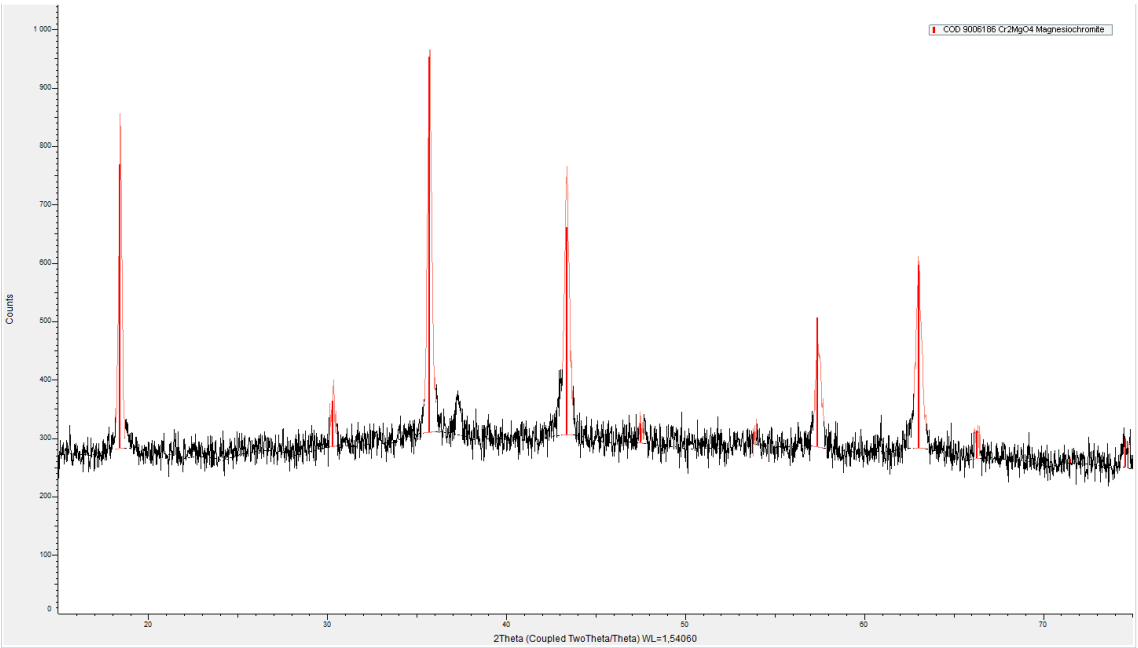

Figure A.3: XRD spectrum of $Cr_2MgO_4 + MgO$ made by sol-gel synthesis

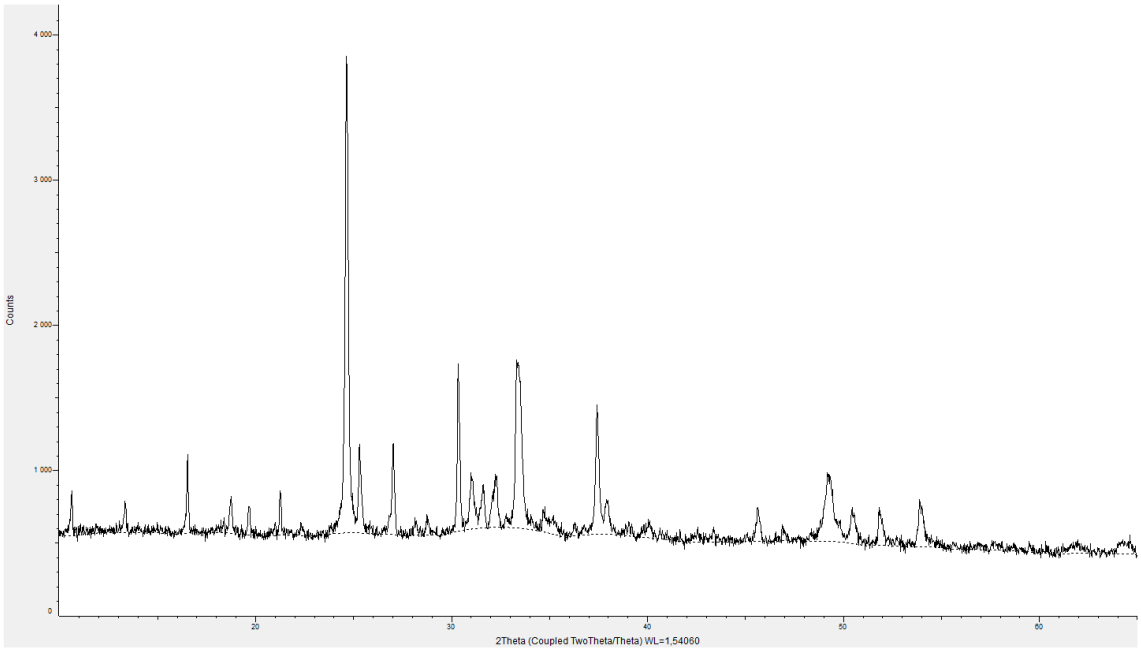

Figure A.4: XRD spectrum of system 1 made by sol-gel synthesis during the first try

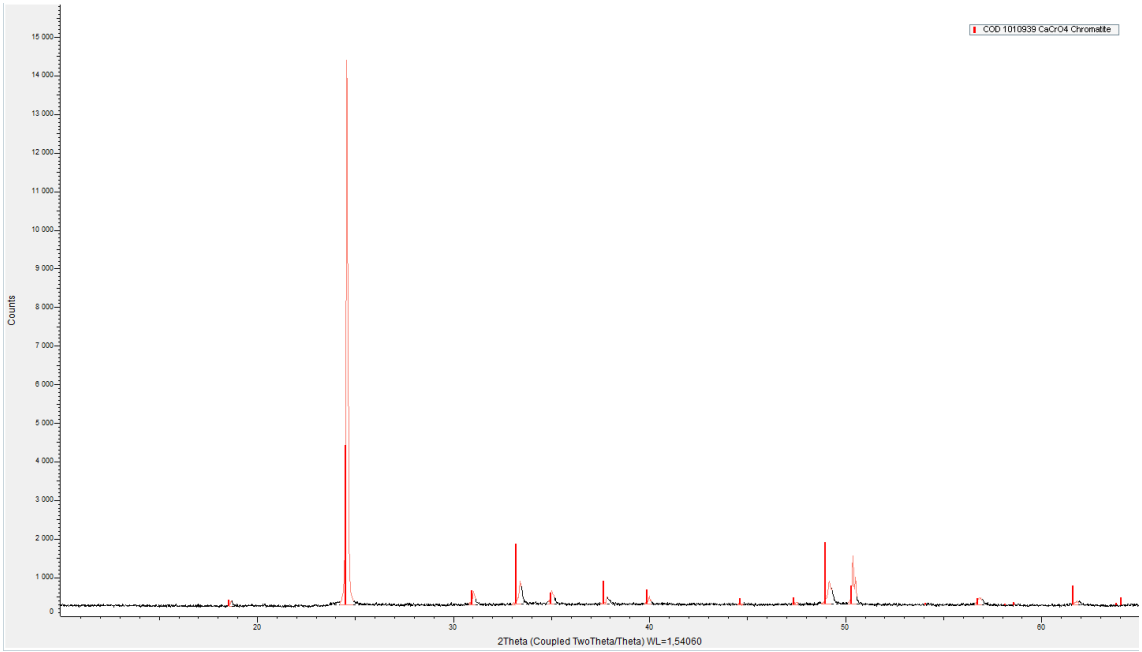

Figure A.5: XRD spectrum system 1 made by sol-gel synthesis during the second try

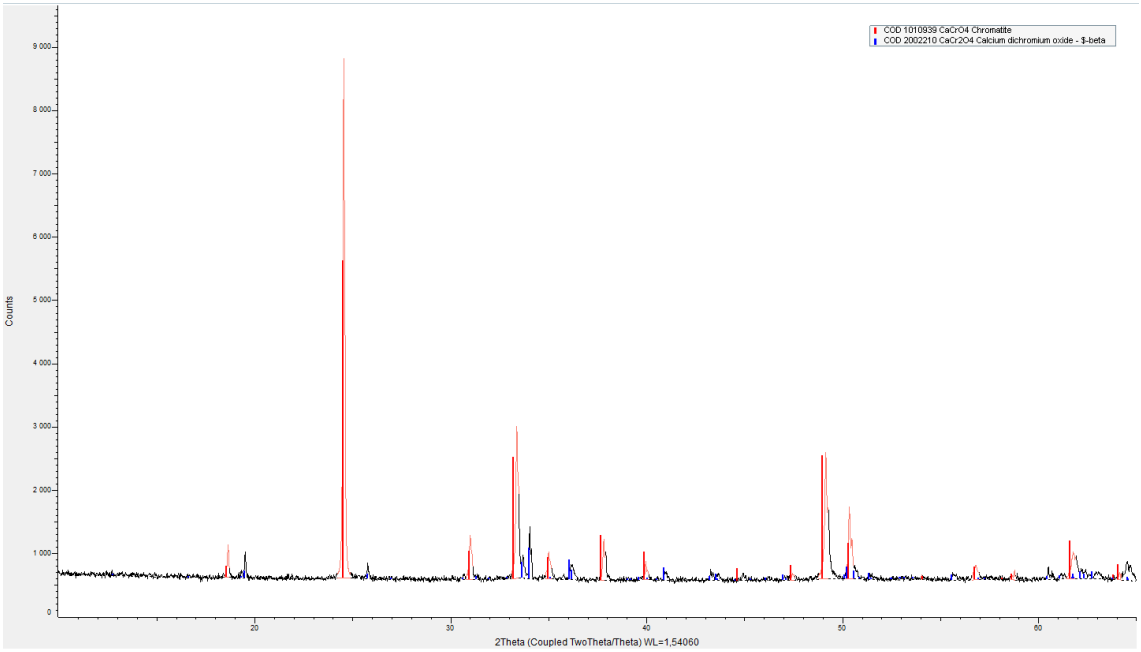

Figure A.6: XRD spectrum of system 1 made by solid state synthesis

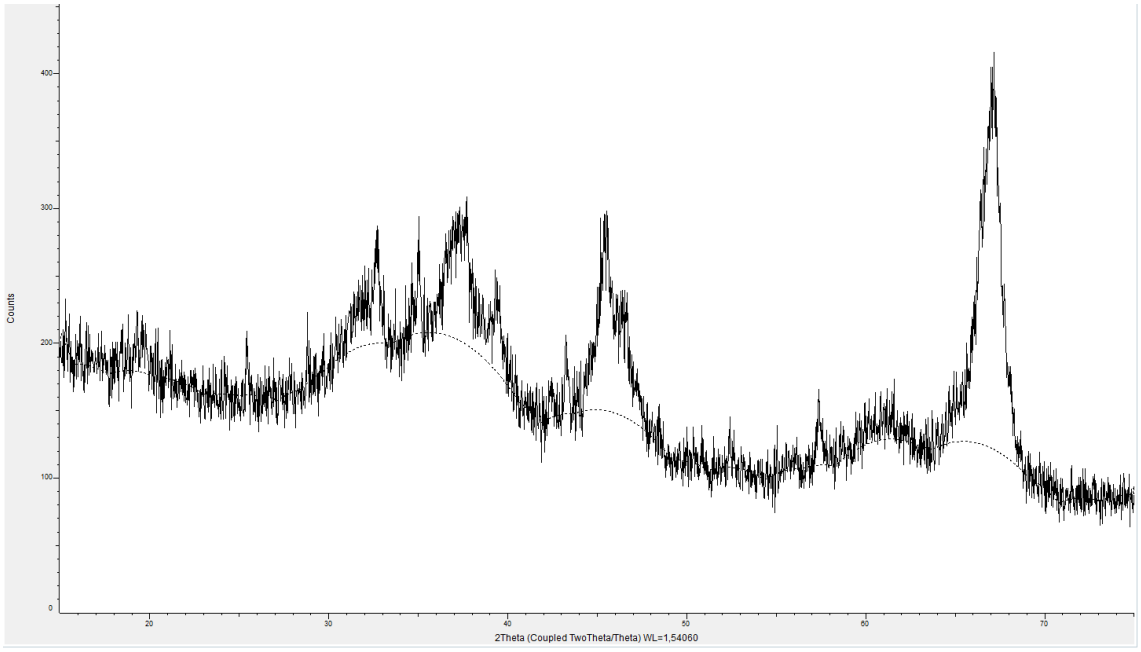

Figure A.7: XRD spectrum of $AlLiO_2$ made by solid state synthesis

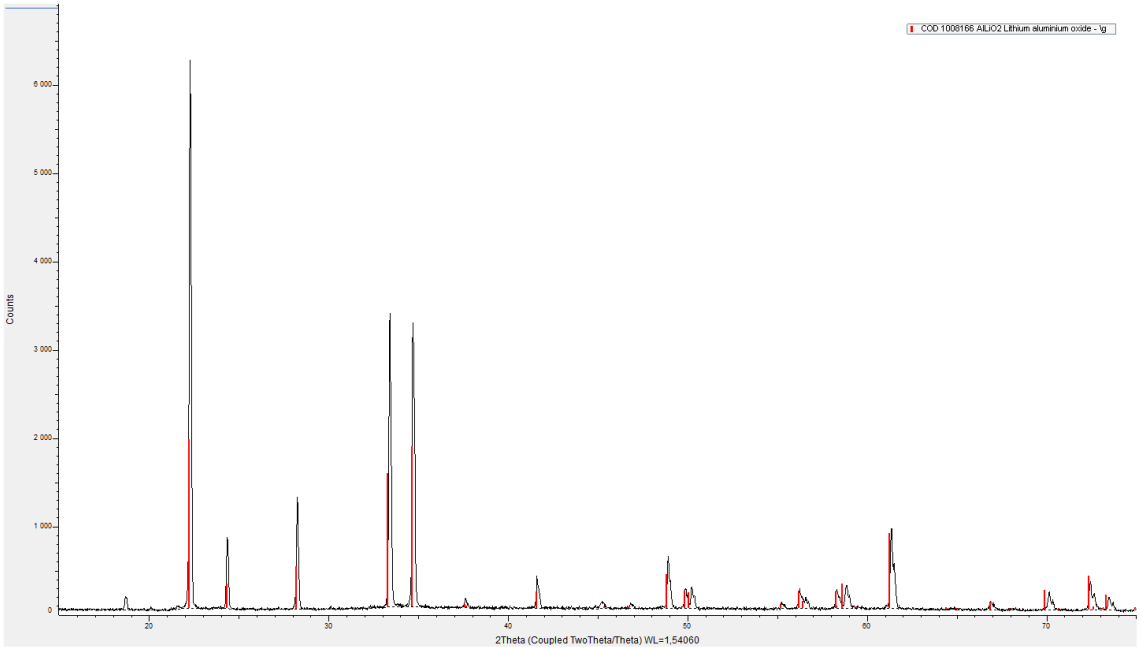

Figure A.8: XRD spectrum of $AlLiO_2$ made by sol-gel synthesis

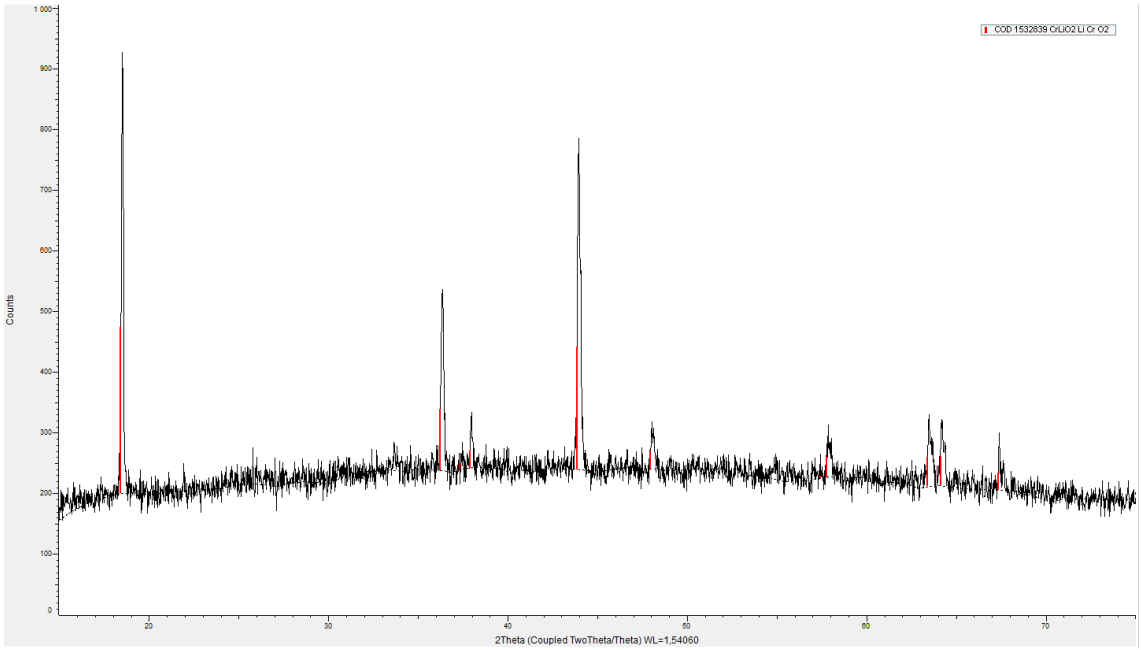

Figure A.9: XRD spectrum of $CrLiO_2$ made by sol-gel synthesis

DEPARTMENT OF CHEMISTRY AND CHEMICAL ENGINEERING
CHALMERS UNIVERSITY OF TECHNOLOGY
Gothenburg, Sweden
www.chalmers.se

CHALMERS
UNIVERSITY OF TECHNOLOGY